**Kaunas University of Technology**

Faculty of Mechanical Engineering and Design

# Compliant Bicycle Spoke for In-Wheel Suspension

Master's Final Degree Project

**Prathmesh Hitesh Shah**

Project author

**Assoc. prof. dr. Inga Skiedraitė**

Supervisor

**Kaunas, 2026**

**Kaunas University of Technology**
Faculty of Mechanical Engineering and Design

# Compliant Bicycle Spoke for In-Wheel Suspension

Master's Final Degree Project
Mechanical Engineering (6211EX009)

**Prathmesh Hitesh Shah**
Project author

**Assoc. prof. dr. Inga Skiedraitė**
Supervisor

**Assoc. prof. dr. Saulius Diliūnas**
Reviewer

**Kaunas, 2026**

**Kaunas University of Technology**

Faculty of Mechanical Engineering and Design

Prathmesh Hitesh Shah

# Compliant Bicycle Spoke for In-Wheel Suspension

## Declaration of Academic Integrity

I confirm the following:

1. I have prepared the final degree project independently and honestly without any violations of the copyrights or other rights of others, following the provisions of the Law on Copyrights and Related Rights of the Republic of Lithuania, the Regulations on the Management and Transfer of Intellectual Property of Kaunas University of Technology (hereinafter – University) and the ethical requirements stipulated by the Code of Academic Ethics of the University;

2. All the data and research results provided in the final degree project are correct and obtained legally; none of the parts of this project are plagiarised from any printed or electronic sources; all the quotations and references provided in the text of the final degree project are indicated in the list of references;

3. I have not paid anyone any monetary funds for the final degree project or the parts thereof unless required by the law;

4. I understand that in the case of any discovery of the fact of dishonesty or violation of any rights of others, the academic penalties will be imposed on me under the procedure applied at the University; I will be expelled from the University and my final degree project can be submitted to the Office of the Ombudsperson for Academic Ethics and Procedures in the examination of a possible violation of academic ethics.

Prathmesh Hitesh Shah

*Confirmed electronically*

**Kaunas University of Technology**

Faculty of Mechanical Engineering and Design

# 1. Task of the Master's Final Degree Project

**Given to the student** – Prathmesh Hitesh Shah

## 1. Topic of the project

Compliant Bicycle Spoke for In-Wheel Suspension

*(In English)*

Paslankus dviračio stipinas ratlankio pakabos sistemoje

*(In Lithuanian)*

## 2. Aim and tasks of the project

Aim: to develop a new compliant spoke design that delivers hub radial deflection under a clearly defined vertical load case, while maintaining wheel structural stability with simulation and experimental validation.
Tasks:
1. to define the wheel-spoke performance requirements, load cases, test protocol, and benchmark metrics for evaluating in-wheel suspension and stability;
2. to create and parametrize a new compliant spoke architecture and interfaces (hub/rim) as a build-ready CAD product definition;
3. to optimize and verify the design via simulation to achieve hub deflection while retaining rim geometry and meeting strength/stability constraints;
4. to manufacture prototypes and experimentally validate hub deflection and wheel stability, and correlate experimental results with simulation;
5. to compare the final design against existing spoke/wheel solutions and deliver a cost–manufacturing–feasibility evaluation with final design guidelines.

## 3. Main requirements and conditions

The developed compliant spoke shall achieve hub radial deflection ≥ 10 mm under a clearly defined vertical load case. The wheel shall remain stable under equivalent "wheel+rider" loading, expected total mass of 80 kg, with no permanent deformation and rim geometry retained within the specified tolerance. The final result shall be supported by FEA simulation and experimental testing using consistent load cases and metrics.

## 4. Additional requirements and conditions for the project, report and appendices

Not applicable.

| | | | |
|---|---|---|---|
| Project author | Prathmesh Hitesh Shah | | 2026-02-11 |
| | *(Name, Surname)* | *(Signature)* | *(Date)* |
| Supervisor | Inga Skiedraitė | | 2026-02-11 |
| | *(Name, Surname)* | *(Signature)* | *(Date)* |
| Head of study field programs | Kęstutis Pilkauskas | | 2026-02-11 |
| | *(Name, Surname)* | *(Signature)* | *(Date)* |

Shah, Prathmesh Hitesh. Compliant Bicycle Spoke for In-Wheel Suspension. Master's Final Degree Project / supervisor Assoc. prof. dr. Inga Skiedraitė; Faculty of Mechanical Engineering and Design, Kaunas University of Technology.

Study field and area (study field group): Mechanical Engineering, Engineering Sciences

Keywords: Chinese finger trap, compliant bicycle spoke, in-wheel suspension, stiffness, buckling resistance, pretension

Kaunas, 2026. 64 p.

## Summary

In this study, a new hybrid compliant in-wheel micro-suspension, inspired by the Chinese finger trap (CFT), was developed and tested. The research problem was identified as the limited radial compliance of the conventional tensioned bicycle spokes, as well as the instability that was experienced when a full-length CFT structure was used as a spoke-like element in the past. The validated nonlinear compliance of the CFT mechanism was reformulated in a hybrid coaxial architecture, applying a staged engineering design methodology. In this architecture, compliant regions, which were derived from CFT, were integrated locally with coaxial tube sections for support, alignment, installed stiffness, and buckling resistance. The design was evaluated for an 80 kg bicycle-rider system, a 675 N screened service load, a maximum service hub deflection of 2.50 mm and a minimum impact hub deflection target of 10 mm. The 29,400 profiles were screened with a parametric MATLAB process to evaluate their geometric admissibility, installed-state support, branch-force participation, service-state feasibility, spoke-count requirement, buckling safety and impact-response. There were just four profiles that met the full thesis criteria, which indicates that the feasible design region was very small. The profiles 7376 and 13224 were then realized in CAD and evaluated using the SolidWorks component simulations. Profile 7376 was determined to be the compliance oriented candidate with 14.54 mm predicted impact hub deflection and 20.87 mm lock margin. The support oriented candidate, profile 13224, was determined to have 0.95 mm deflection at the service hub, 10.00 mm deflection at the impact hub, and was deemed to be a viable 20-spoke configuration. Experimental observations verified the nonlinear stiffening behaviour of the CFT mechanism, and the importance of branch-load balance to the durability of the hybrids was also found. The hybrid CFT spoke was determined not to be a commercial ready component, but a validated design pathway was set in place to move a compliant mechanism to a wheel relevant spoke architecture.

Shah, Prathmesh Hitesh. Paslankus dviračio stipinas ratlankio pakabos sistemoje. Magistro baigiamasis projektas / vadovė doc. dr. Inga Skiedraitė; Kauno technologijos universitetas, Mechanikos inžinerijos ir dizaino fakultetas.

Studijų kryptis ir sritis (studijų krypčių grupė): Mechanikos inžinerija, Inžinerijos moklslai.

Reikšminiai žodžiai: kinų pirštų gaudyklė, paslankus dviračio stipinas, pakaba rate, standumas, atsparumas išlinkimui, įtempimas.

Kaunas, 2026. 64 p.

## Santrauka

Šiame tyrime buvo sukurta ir išbandyta nauja hibridinė, suderinama rato viduje esanti mikropakabos sistema, įkvėpta kinų pirštų gaudyklės (CFT). Tyrimo problema buvo įvardyta kaip ribotas įprastų įtemptų dviračių stipinų radialinis lankstumas, taip pat nestabilumas, kuris buvo patiriamas, kai stipinų formos elementas buvo vientisa CFT konstrukcija. Patvirtintas netiesinis CFT mechanizmo suderinamumas buvo suformuluotas hibridinėje bendraašėje architektūroje, pagrindžiant inžinerinio projektavimo metodikos etapais. Šioje architektūroje iš CFT gautos suderinamos sritys buvo lokaliai integruotos su bendraašėmis vamzdžių dalimis, kad užtikrinti atramą, centravimą, montavimo standumą bei atsparumą išlinkimui. Konstrukcijai vertinti buvo pasirinkta 80 kg sveriančią dviračio–dviratininko sistema, esant 675 N apkrovai, bei maksimalią 2,50 mm darbinės stebulės deformacijai ir minimaliai 10 mm smūginės stebulės deformacijai. 29 400 profilių buvo patikrinti naudojant MATLAB procesą, siekiant įvertinti jų geometrinį priimtinumą, atramą sumontuotoje būsenoje, šakų jėgos dalyvavimą, tinkamumą eksploatacinėje būsenoje, stipinų skaičiaus reikalavimą, išlinkimo saugumą ir smūgio reakciją. Buvo tik keturi profiliai, kurie atitiko visus tyrimo kriterijus, o tai rodo, kad galimas projektavimo regionas buvo labai mažas. Profiliai 7376 ir 13224 buvo realizuoti CAD programoje ir įvertinti naudojant „SolidWorks“ komponentų modeliavimą. Profilis 7376 buvo nustatytas kaip atitinkantis paslankumo reikalavimus, kur numatoma smūginės stebulės deformacija yra 14,54 mm, o fiksavimo atsarga – 20,87 mm. Nustatyta, kad į atramą orientuotas profilis 13224 turi 0,95 mm nuokrypį stebulėje ir 10,00 mm nuokrypį esant smūgiui stebulėje, ir buvo laikomas tinkamiausia 20 stipinų konfigūracija. Eksperimentiniai stebėjimai patvirtino netiesinį standėjimą CFT mechanizme, taip pat nustatyta šakų apkrovos balanso svarba hibridų ilgaamžiškumui. Hibridinis CFT stipinas nėra komercinė gamybai paruoštas komponentas, jis buvo sukurtas, kad įrodyti, kad galima pritaikyti paslankų mechanizmą dviračio rato stipinams.

## Table of contents

## List of figures

## List of tables

## Introduction

A bicycle wheel is not a single component, but a prestressed structural system, the stiffness, stability, and dynamic response of which is due to the interplay of the rim, hub, spokes, tyre, and the interface with the terrain. It is this view that underpins the current work, since the concept of a bicycle speaking in a very compliant way cannot be affected at the expense of other compliance that may be introduced without interfering with the structural roles enabling the wheel to be worked safely and efficiently. The traditional wire-spoke wheel is a highly effective loading structure; it has an extremely limited vertical complacency, in the sense of suspension travel. Radial loading of the wheel causes mainly local tension decreases in the spokes adjacent to the contact zone, whereas the pretensioned spoke network maintains a lightweight, stiff, and torsionally viable structure with comparatively minor deformations in normal service environments. Consequently, it is the pneumatic tyre, in combination with compliance elsewhere in the bicycle-rider system, which provides most comfort related deformation in a conventional bicycle.

Though structurally effective as well as economical, its inherent compliance has been limited, driven to create other comfort-enhancing mechanisms, including suspension forks, rear suspension units, and other damping devices. Such solutions have the potential to make riding more comfortable, yet generally add to mass, cost, and maintenance demands. Simultaneously, engineering design has sought more and more lightly and highly integrated systems by using material efficient structures, modular design, and compliant mechanisms. Herein this general framework, compliant structures provide a potential pathway to directly incorporate regulated elastic behaviour into a component without affecting mechanical performance and structural integrity.

The engineering task covered in this research arises when in-wheel suspension is not considered as a new product segment or a wheel design, but rather, as a structural design requirement at the spoke level. It aims to ensure that impressive radial hub deflection can take place under a prescribed vertical load condition with the wheel still being supported, the rim maintaining its positional stability, and the elastic integrity. The load case achieving this in this work is a minimum radial hub deflection of 10 mm with an 80 kg bicycle-and-rider load case, without any deformation being permanent and without any aversion of the structural functionality of the wheel being intolerable. This is both a challenging design problem, as compliance and stability cannot be implemented independently of one another.

The research is based on previous works where a full-length Chinese finger trap (CFT) helical lattice spoke was developed, designed, manufactured, and tested experimentally to test the effect of necking, unstable deformation, and squeegee behaviour. The previous stage demonstrated the CFT as a feasible compliant system which also identified the practical constraints of an entirely compliant complete spoke especially in terms of structural stability and buckling. It can be planned as taking the current concept to the next stage of mechanism validation to wheel-relevant design development with the introduction of a new compliant spoke architecture to preserve the desirable nonlinear behaviour of the CFT but to enhance structural stability and spoke-ability.

As such, the research does not have the restriction of proving that a compliant mechanism will deform under load. It is designed to create a concept spoke that can serve as both a structural wheel element and also offer helpful compliance. To realize this, the study is a synthesis of requirement definition, parametric design, numerical screening, structural simulation and experimental reasoning into a unit

design-development framework. so that it can fill the gap between compliant mechanism theory and the practical in-wheel shock-absorption spoke design.

Aim: to develop a new compliant spoke design that delivers hub radial deflection under a clearly defined vertical load case, while maintaining wheel structural stability with simulation and experimental validation.

Tasks:

1. to define the wheel-spoke performance requirements, load cases, test protocol, and benchmark metrics for evaluating in-wheel suspension and stability;
2. to create and parametrize a new compliant spoke architecture and interfaces as a build-ready CAD product definition;
3. to optimise and verify the design via simulation to achieve hub deflection while retaining rim geometry and meeting strength/stability constraints;
4. to manufacture prototypes and experimentally validate hub deflection and wheel stability, and correlate experimental results with simulation;
5. to compare the final design against existing spoke/wheel solutions and deliver a cost-manufacturing-feasibility evaluation of the final design guidelines.

Hypothesis: A compliant spoke design can achieve significant radial deflection under vertical loading while maintaining the structural stability and elastic integrity of the wheel assembly within defined material limits.

# 1. Theoretical Background

## 1.1. Bicycle Wheel Mechanics, Spoke Functions, and Motivation for In-Wheel Compliance

A bicycle wheel is a complex system of prestressed structural elements, rather than the simple assembly of discrete parts it is often perceived as. The load carrying capacity and mechanical behaviour arise from the interactions between the rim, hub, spokes, tyre and ground contact. In essence, the network of tensioned spokes connecting the rim and the hub holds the wheel together. When a radial load is applied, the active spokes adjacent to the contact region experience a minor compression component resulting in reduced pretension compared to the initial installed state, while the rest of the network contributes to preserving the wheel shape along with the rim, as shown in Fig. 1 [1-3]. This is the working principle and the major reason why the bicycle wheel exhibits high load-bearing efficiency while remaining lightweight [2, 3].

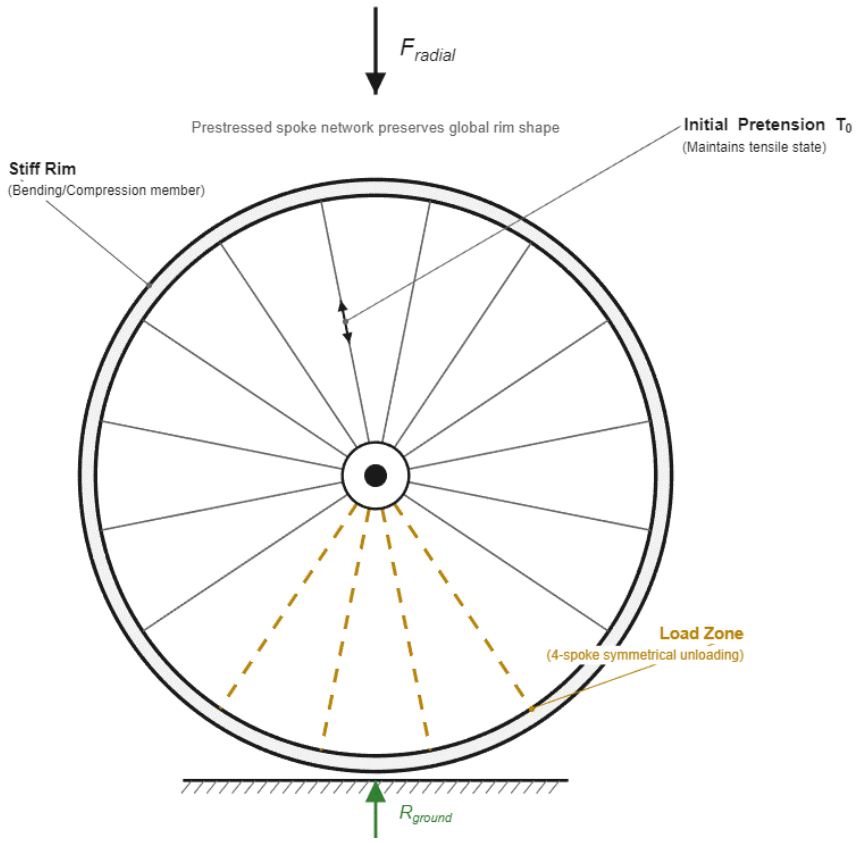


**Fig. 1.** Schematic of a conventional bicycle wheel under radial load [3]

The same efficient design also exposes limitations that are vital to the present research. A traditional spoke is optimised to work as a network of tensioned elements, demanding support, stiffness and mass efficiency from each element. This highly stiff nature and pretension work principle limits the flexure a lightweight structure can exhibit, resulting in very little radial travel at the spoke level. This compliance free design focus of spokes removes expectations of any shock-absorption or any damping occurring at the hub level due to spokes. Under normal service conditions, most comfort related compliance is obtained from pneumatic tyre and standalone systems like suspensions or dampers in the rest of the bicycle-rider system [4-7]. As demonstrated in multiple analytical and experimental studies, radial stiffness in a bicycle wheel is not governed by individual spoke stiffness alone but has multiple contributors like spoke preload, rim bending stiffness, spoke layout and count,

and load distribution across the wheel [3, 8, 9]. With this insight, given than a spoke governs multiple aspects of wheel performance, any attempt to introduce compliance at spoke level must adhere to preserving the structural logic for a wheel rather than treating a spoke as an isolated spring-like element [1, 3, 8].

When durability is considered, the point is even more important, Gavin showed that spokes must separately be evaluated for their fatigue sensitive service conditions which it is linked to spoke behaviour as they are repeatedly loaded structural members. Any structure under consideration for spoke replacement must be carefully examined for its structural function, cyclic loading and long-term preservation of wheel behaviour rather, as they are allowed to deform significantly [10].

The complexity associated with the introduction of compliance at spoke-level in a bicycle wheel is far more complex than simply reducing spoke stiffness. Any proposed solution for a compliant spoke design must be capable of delivering meaningful radial travel compared to pneumatic tyre level compliance under a prescribed vertical load while maintaining compatibility with the structural requirements imposed on spokes within a bicycle wheel. Any structure that fails to maintain sufficient support, buckles or exhausts its compliance capacity prematurely while undergoing deformation is not useful. Conversely, a spoke that can provide all the structural stability and remains perfectly stable but produces negligible hub travel does not satisfy the product requirement based on its intended in-wheel suspension function and cannot qualify as an acceptable solution [1-3, 10]. This highlights an engineering gap in the domain of in-wheel suspension functionality, delivered via compliance in spoke architecture, which forms the core motivation for the research. The overall design problem is inherently a combination of compliance, installed state support, stability and wheel level relevance.

### 1.2. Compliant Mechanisms and Existing In-Wheel Compliance Concepts

The primary structural role played by conventional bicycle spoke is to act as tensioned members within a prestressed wheel system, not intended to provide large recoverable radial travel, meaning excessive local compliance is normally not desired. This results in problems with introduction of spoke level compliance is better comprehended as a compliant mechanism design than as a simple material substitution problem. Compliant mechanisms in essence are generation of useful motion through elastically controlled deformation by replacing traditional rigid joints in the system, where deformation is controlled, directional, recoverable and structurally useful [11, 12].

This distinction is crucial as the design objective is to encapsulate a load path element that deforms purposefully, directionally and recoverable under wheel loading rather than merely using a softer material for the spoke. The compliance must be intentional, mechanically useful and compatible with the support function of the wheel, while preserving meaningful structural support and not simply be flexible in all directions. Reviews on the synthesis of compliant mechanism emphasise that geometry, topology and structural arrangement provide more sensitive control over the stiffness and motion output as compared to bulk material choice alone [11, 12].

Existing in-wheel compliance concepts demonstrate multiple engineering challenges occurring when integrating suspension like behaviour into the wheel itself. Studies involving bicycles equipped with in-wheel suspensions demonstrate the wheel integrated compliance can be analysed in both dynamic and experimental terms rather than treated as a prospective idea [13]. Another research showed that in-wheel suspension can reduce the transmitted vibration and improve comfort factor in the overall riding experience [14]. These researches shows that the wheel is a valid location for the added

suspension functionality, at the same time such system must be judged at the system level rather than only by a local component deformation [13, 14].

Most existing compliant wheel, commercialised concepts reinforce the points mentioned above. Loopwheels replace traditional spoke network solution with compliant loop elements that allow relative motion between hub and rim while still maintaining wheel function [15]. SoftWheels another example of commercial compliant solution, follows a similar wheel level compliance objective, achieving this by using a complex internal suspension architecture for the controlled hub movement [16]. Both examples are vital to the study as they lay foundational work on not just the possibility of compliance in-wheel systems but provide fresh perspectives and techniques to overcome the same objectives, meaningful controlled hub travel while preserving the wheel overall as a system and its functionality. A common limitation observed in both products is that in order to achieve a functional system, they achieve the increased compliance by a wheel-level redesign not through development of structurally disciplined compliant spoke, which is the core of the following research, a spoke originated compliance for in-wheel suspension [13, 15, 16].

Compliance achieved through alternative spoke material follows a different line of products. Spinergy introduced PBO spoke systems, while Berd developed UHMWPE spokes as solution targeting reduced rotating mass and altered, enhanced, ride feel. These solutions operating on similar principles provide another perspective, eliminating the dependency on traditional stainless-steel spokes in order to have a structurally functional wheel. They suggested that reduced mass, increased damping and change in ride experience can be achieved within the spoke domain, however they still remain fundamentally close to the tension member principle. Still being tensioned spokes primarily, their take on compliance with woven and braided structures with integration of alternative materials, architected compliant mechanisms intended to generate substantial and controlled hub travel [17-19].

The spoke like compliant structural concepts, are not just limited to conventional bicycle spoke domain. Some researchers have examined wheel with flexible spokes, while another aspect studied was a non-pneumatic tyre with V-shaped spoke like members. Both domains remain relevant as they explore spoke elements and show such elements can strongly influence radial deformation, hub deflection, stiffness and structural support. In other words, the spoke is not always a passive connector, under the correct geometric conditions, spoke like members can still become the primary contributors for wheel level compliance [20, 21].

A common pattern observed across all studies is, conventional spokes are structurally efficient but not designed for meaningful suspension like travel summarised in Table 1. Existing commercial products, focused on compliant wheel system, demonstrate that wheel level hub movement is feasible, but typically achieved through a full system redesign. Additionally, compliance is not strictly obtained via geometric optimisation, but also open to innovative solutions integrating alternative spoke material, though it largely operates on the tensioned member principle. Flexible spoke inspired structural concepts reveal that geometry driven compliance is possible, but do not solve the problem themselves of spoke level structural discipline. This supports the objectives targeted through this research, achieving compliance which is introduced deliberately and locally while providing support and stability cannot be obtained alone by softer conventional spokes or a complete wheel redesign, but a hybrid spoke architecture remains a promising route [11-13, 15-21].

**Table 1.** Existing compliance strategies and their limitations

| Concept | Compliance location | Structural principle | Expected hub travel | Main Limitations |
|---|---|---|---|---|
| Conventional wire-spoked bicycle wheel | Tyre and minor system-level compliance; spokes remain primarily tension members | Prestressed spoke network supports the rim through tensile spokes and load redistribution | Very low at spoke level | Structurally efficient, but does not provide meaningful spoke-level suspension travel |
| Wheel-level compliant suspension concepts | Compliance integrated at wheel level between hub and rim | Wheel architecture redesigned so that hub-rim relative motion is allowed while preserving global function | Moderate to high | Demonstrates feasibility of wheel-integrated compliance, but usually requires full system redesign rather than a spoke-like structural solution |
| Loopwheel-type concept | Hub-to-rim compliance through composite loop elements replacing conventional spokes | Deformable loop elements provide controlled radial motion and shock absorption | High | Achieves real hub travel, but departs significantly from the structural logic of a conventional spoke-based wheel |
| SoftWheel-type concept | Internal wheel-level suspension mechanism between hub and rim | Internal suspension architecture enables controlled hub movement under load | High | Effective as wheel-integrated suspension, but mechanically more complex, bulkier, and less representative of a spoke-level compliant architecture |
| Alternative fibre-spoke systems (e.g., PBO, UHMWPE) | Spoke domain | Conventional tension-member logic retained, but with lower mass and altered damping/ride feel through material substitution | Low to modest | Shows that spoke materials can be innovated, but remains fundamentally close to the conventional tension-spoke paradigm and does not provide large controlled hub travel |

### 1.3. Chinese Finger Trap as Potential Compliant Mechanism for Spoke Applications

Chinese finger trap (CFT) is a special case of helical lattice pattern structure in which axial deformation is intricately coupled with radial deformation. The ability to optimise the structure primarily through geometry and internal configuration to achieve controlled compliance rather than through simple material softening makes it a structure worth investigating for spoke application. This makes the CFT structure particularly relevant to the spoke design, as it offers fine tuning for controlled deformation, stiffness variation and lock up behaviour through geometric manipulation which can later be complimented by material substitution providing enhanced output [22-27].

This set of helical lattice structures was also reinforced by other research works, in which Dixon found that helical lattice structures can have tailored elasticity, Carey showed that helical architectures can rearrange through controlled topological reconfigurations and Quaglierini studied the mechanics of tubular networks of elastic helical fibres [22-26]. Evidence that helical lattice structures are not just mathematically dominated, but also highly mechanically controlled, systems whose response is controlled as much by the structure as by the material.

A more focused and specialised research on the CFT structure alone gives insights into the governing properties and critical structure considerations that must be obeyed when designing for specific application. Research by Lu and team [27] shows that radius, pitch, helix angle, turn count and strip

width are strongly connected and that the CFT possesses a critical width criterion for geometric admissibility for practically possible designs as shown in Fig. 2.

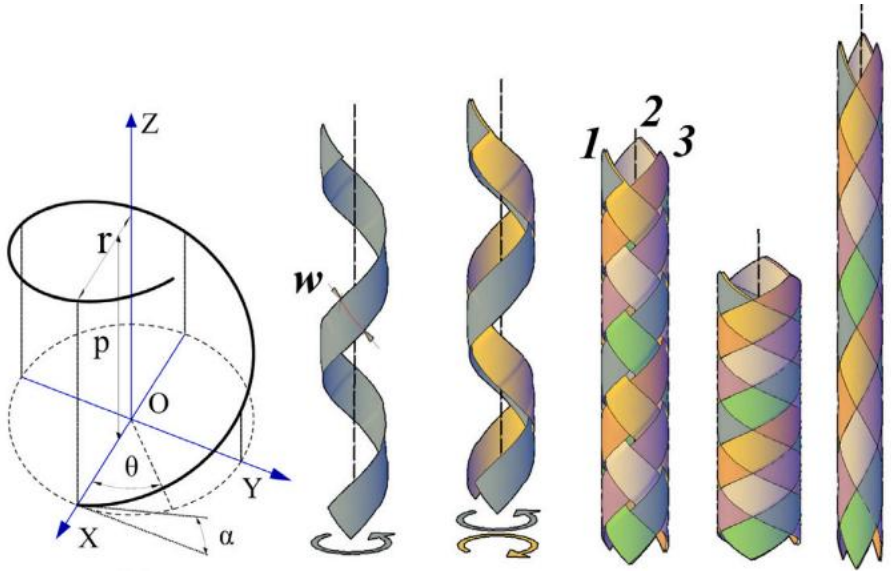


**Fig. 2.** Design of Chinese finger trap [27]

The paper also shared insights on a property called “Necking” where the end radii are constrained and fixed as displayed in Fig. 3, due to which the structure develops the nonlinear relation, which ties the axial deformation to the radial deformation, also resulting the force-displacement to have a strongly nonlinear response [27].

**Fig. 3.** Necking of CFT [27]

This ability of the CFT structure to generate nonlinear mechanical behaviour without requiring unusual assumptions, because majority of this response arises from geometric reconfiguration. That means, stiffness and deformation range can, in principle, be fine-tuned by design variables such as strip width, strip thickness, turn count, initial height, etc as shown in Fig. 2. The same geometric correlations make the CFT structure a design challenge, where feasibility, local curvature,

deformation range, lock-up behaviour, and stiffness all change together and must be taken in consideration while in development.

Preceding research depicts that a CFT structure can provide controlled optimisation on factors such as deformation, stiffness, etc, which are the properties ideal for a compliant spoke mechanism. This nonlinear compliance is useful, but a full length CFT structure, cannot be treated as a complete spoke itself, due to stability issues given lack of directional deformation, buckling. However, this provides a foundation for the concept of localised compliance, with CFT structure giving control over the compliant regime and a stability element working together in a complete hybrid architecture addressing the structural limitations [27, 28].

### 1.4. From Full-length Compliant Spoke to Hybrid Architecture: Stability, Buckling, and Structural Refinement

A concept of full-length compliant structure inspired by a Chinese finger trap was designed, modelled, manufactured and experimentally tested as a mechanism level proof of concept. Earlier research demonstrated that the unique helical structure of CFT geometry can produce nonlinear deformation behaviour, necking and progressive stiffening, these properties and overall mechanism was validated experimentally.

At the same time, the earlier project also showed that a fully compliant spoke extending across the complete hub to rim span lacked sufficient structural discipline and was vulnerable to instability and buckling. A structure can be considered truly a spoke replacement when it is a mechanically strong geometry providing compliance but without compromising the structural stability of the bicycle wheel itself, is it vital to understand the difference between the mechanism validity and the overall feasibility of the spoke replacement structure. Making the full-length CFT concept as an experimentally validated mechanically compliant structure, starting ground for the design optimisation [11, 27].

Howell in his work explains the need for partial-compliance, regional or divided by components, allowing the structure to provide controlled deformation and load bearing functionalities. In such cases, compliance is localized within selective elements of the system, while the other elements work towards providing support and stability. In conclusion, instead of allowing the entire spoke to behave as one compliant lattice, it would be beneficial to design localised compliance into CFT-derived regions and introduce a hybrid model that improves axial guidance and buckling resistance [11].

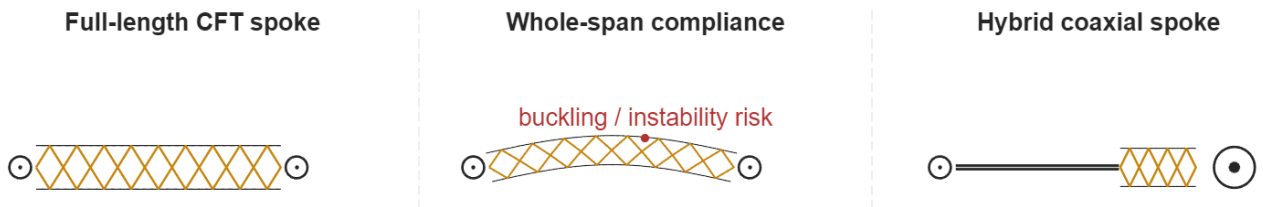


**Fig. 4.** Structures of spokes [11]

As the direct consequence of the earlier mechanism-level validation and of the structural limitations exposed by that earlier work represented by a simplified Fig. 4. The hybrid architecture is intended to preserve the useful nonlinear compliance of the CFT while addressing the spoke-level requirements

that the full-length concept could not meet, particularly installed-state support, buckling resistance, and wheel-relevant structural discipline, summarised in Table 2 [11, 27].

**Table 2.** Summary of requirements

| Concept | Compliance location | Structural principle | Main strength | Main limitations |
|---|---|---|---|---|
| Full-length CFT spoke (preceding project) | Entire spoke span | Whole-span compliant helical lattice | Validated geometry-driven nonlinear compliance and necking-type behaviour | Insufficient structural discipline over full span; vulnerable to instability and buckling |
| Hybrid coaxial spoke (present study) | Localized CFT-derived region | Compliance combined with a stabilizing coaxial structural span | Preserves useful compliance while improving spoke-like support and stability | Requires detailed screening, branch-balance control, and validation of load sharing |

## 1.5. Modelling and Validation Approaches Used in Related Work

Analytical modelling is useful for identifying governing geometric relations and for screening designs based on admissibility limits, but it cannot capture every interface effect or structural detail. Reduced order numerical filtering allows large parameter space to be explored efficiently, though it simplifies contact, anisotropy and full wheel interaction. With the numerical filter, CAD and FEA process can be streamlined selectively for the profiles that are shortlisted to be interpreted as real concepts with stress concentrations and interfaces, avoiding the inefficiency of doing it for a larger design sample space. Experimental work provides the strongest physical validation, but is associated with the fabrication effort, cost and time, reserved for the selected profile.

This staged logic is also consistent with prior bicycle-wheel research. Salamon and Oldham highlighted the practical importance of numerical modelling for bicycle-wheel design, while Mínguez and Vogwell showed that even simplified analytical treatments can provide useful insight into radial stiffness and spoke load distribution. Corno extended this broader logic to the problem of in-wheel suspension, reinforcing the idea that wheel-integrated compliance should be approached through a layered combination of modelling and interpretation rather than through a single isolated method [8, 9, 13].

Printed PLA and CF-PLA are useful for repeatable prototyping and mechanism validation, but studies on fused-deposition manufactured carbon-fibre-reinforced PLA show clearly that gains in stiffness do not automatically translate into equally strong gains in strength or durability, and that the final response remains strongly dependent on print conditions. This means that prototype materials are useful for validating architectural and mechanism behaviour but should not be treated as direct evidence of production-level spoke performance [29, 30].

Technical data for PBO, CFRP and UHMWPE indicates that high performance fibre systems may be more relevant than printed polymers for commercial spoke implementation. Simultaneously, their behaviour is directional and manufacturing process sensitive, which justifies the use of simplified or equivalent descriptions during early-stage screening when the purpose is to isolate geometry driven progression [29-33].

The validation logic adopted in the present work is therefore well supported by the literature and the project scope. MATLAB screening reduces a large and strongly connected design space to a

manageable shortlist. CAD modelling allows those shortlisted profiles to be interpreted as real spoke like components. Static simulation then tests whether the shortlisted architectures remain mechanically credible. Experimental work validates the hybrid structure mechanism. For research positioned between compliant-mechanism validation and spoke-level wheel design, this layered strategy is the appropriate development path backed by other similar studies [8, 9, 13, 27, 29, 30].

### 1.6. Research Gap

Multiple analysed research works are conclusive and present strong data in several areas individually, but remain weak at point of intersection, presenting the immediate gap for conducting research. Classical bicycle wheel mechanics present details on how prestress, spoke tension, rim support and load redistribution make the conventional wheel structurally efficient [1-3, 8-10]. Comfort and compliance related research works explain why additional wheel level compliance may be desirable [4-7, 13, 14, 34, 35]. Compliant mechanism theory provides the basis for designing meaningful elastic deformation [11, 12, 36, 37]. Helical lattice and Chinese finger trap studies show why such structures are mechanically promising as a geometry driven compliant architecture[22-27]. Material studies indicate possible paths with expected variation in the journey from prototype to eventual production [29-33]. Missing piece of the puzzle is a connected single, disciplined design pathway that brings these strands together in a form directly useful for a spoke level wheel design.

With validation studies proving wheel compliance is possible in a broader sense as well as the fact that a Chinese finger trap can exhibit nonlinear deformation, leaving a gap. The unresolved problem being whether a validated compliant mechanism can be reformulated into a spoke level architecture, that remains sufficiently stable, pretension compatible and wheel relevant to function as a meaningful structural spoke element. Existing fibre spokes remain close to the traditional tension member principle, while compliant wheel products achieve greater hub travel mainly through wheel level system redesign [15-19]. The earlier full length CFT research tried to bridge this gap by validating the mechanism experimentally, but it showed that mechanism validation and architectural validation are not the same.

Proposed research is to addresses the gap by treating CFT not as a complete spoke, but as a localised compliant substructure within a hybrid coaxial architecture. The intended contribution is not a commercialisation ready spoke, rather, it is to establish a technically sound pathway through which validated compliant mechanism can be transitioned towards a wheel relevant spoke concept using geometric admissibility filters, reduced order screening, installed state evaluation, CAD modelling and static structural assessment [11, 27]. The study is expected to form a bridge between compliant mechanism validation and spoke level architectural readiness.

## 2. Methodology

This chapter follows theoretical background and formulation of all the equations used for the development of the design of a compliant lattice patterned, Chinese finger trap inspired spoke for application in bicycle spoke to achieve added functionality of micro-suspension. All the needed equations and steps are explained in this chapter for justification of the iterations in design development.

### 2.1. Research Workflow and Staged Development Logic

This study followed a staged engineering methodology to transform the Chinese finger trap mechanism from a previously validated full-length proof of concept into a wheel-relevant hybrid compliant spoke architecture. The study further develops on the foundation work done in the preceding research where a full-length CFT structure was designed, modelled, fabricated and experimental tested and validated for the geometry driven compliance. CFT structure as a proof of concept when studied in depth revealed the ability of the structure to general geometry driven nonlinear force-deformation relation, resulting in progressive stiffening and large recoverable deformation under constrained conditions. Though the full-length complaint structure also had vulnerabilities, allowing compliance in the full structure makes it susceptible to buckling, as shown in Fig. 5, and less stable in terms of its load bearing capacity, failing to meet the discipline requirements.

**Fig. 5.** Buckling of structure

Further design-based optimisation and refinement of the full-length compliant structure becomes redundant due to lack of axial stability, while affirming the possibility of applying localised compliance within a hybrid coaxial spoke architecture. A hybrid configuration where compliant function is focused, CFT inspired regions, while the coaxial structural components providing stability for the spoke, improving axial guidance, installed-state support and buckling resistance. Resulting in a structure that provides controlled compliance and the ability to fine tune the compliance aspect. This spoke construction is developed by a staged process as shown in Fig. 6, with filters for selecting

the best profiles, based on geometric boundary conditions, installed-state boundary conditions and the target compliance alongside the stiffness configuration that provides needed support as well.

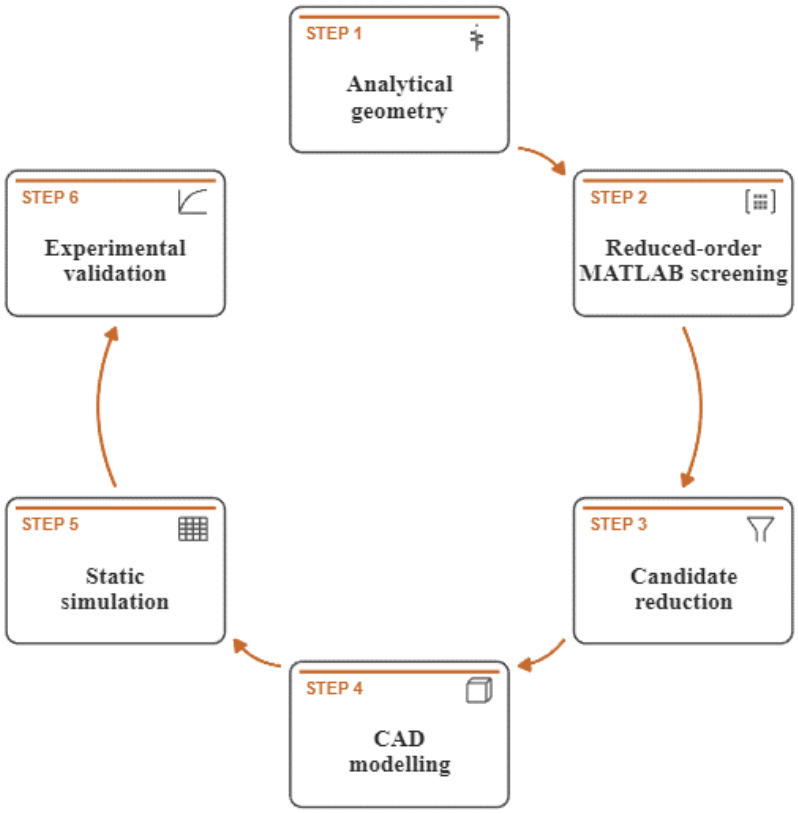


**Fig. 6.** Developing process of spoke

The development process is a linked 6 stage routine. Process starts with the geometric filter, evaluating designs based on admissibility conditions of the CFT structure, due to its geometry driven nonlinear deformation, followed by a simplified MATLAB framework that is used to screen a large sample space under installed-state, service state and impact state. This is used to filter out profiles which fail to meet the required criteria of geometric boundary conditions and different operational states, these shortlisted profiles are then modelled in CAD environment to create a virtual profile meeting all theoretically calculated dimensions. 3D models are then tested under static simulation, to predict expected behaviour under loading conditions, followed by fabrication and experimentally testing under physical loading conditions, to validate predicted behaviour.

## 2.2. CFT Mechanism Principles

Even though the proposed structure is a hybrid coaxial model, the profile sections governing compliance factor remain a CFT mechanism. The CFT section is treated as a constrained helical lattice in which axial extension is accompanied by radial contract due to its nonlinear deformation nature. For a CFT structure when considering the section under a single turn, forms a right-angled triangle as shown in Fig. 7, the geometric relation between radius $r$, single turn strap length $S_1$ and pitch $p$ is given by the Pythagoras theorem as expressed by equation (1):

$$S_1^2 = p^2 + (2\pi r)^2 \quad (1)$$

The interconnected relationship between the geometric dimensions, make it so that axial elongation cause change in the pitch while the strap length is same for a given section causes changes in radius. This varying nonlinear geometry produces a structure that has a controlled deformation range and adaptive stiffness, this is the key distinction compared to a conventional spoke. This compliance is achieved by moderated manipulation of dimensions such as interaction between pitch, radius, turn count, strap width and thickness rather than the material properties alone.

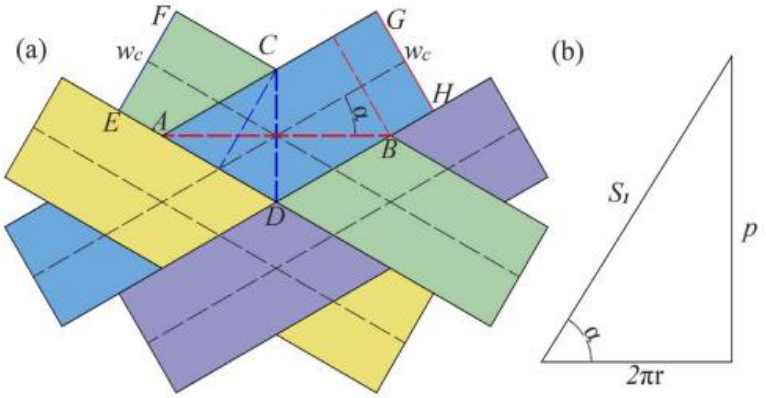


**Fig. 7.** Forms a right-angled triangle of CFT structure

For a given cross-section of the single turn CFT, strap length $S_1$ forms a right-angle triangle with the pitch and the circumference as displayed in Fig. 7. This gives us equation (2) which shows the relation between width, number of strap pairs and circumference and the pitch,

$$wS_1n = 2\pi pr, \tag{2}$$

Combining equations (1) and (2), results in a quadratic equation, where a real root for $p$ exists, such that the critical width $w_c$ can be derived from the determinant of quadratic equation, as shown in equation (3),

$$p^4 - p^2S^2 + (wSn)^2 = 0,\ \Delta = (S^4 - (2wSn)^2 = 0),\ w_c = \frac{S_1}{2n} \tag{3}$$

As the width of the strap approaches the critical width based on the geometric admissibility of the corresponding CFT, the resulting structure becomes more compact, leaving no gaps for deformation, making it a critical dimensional constraint to be optimised for the desired deformation range. The resulting structure with width less than critical width has two extreme deformation configurations, one which is complete compression with ($p_{min}$, $r_{max}$, $\alpha_{min}$) and second, completely elongated with ($p_{max}$, $r_{min}$, $\alpha_{max}$), these extreme conditions can be calculated by equation (4),

$$p_{min/max} = \sqrt{\frac{S^2 \pm \sqrt{\Delta}}{2}}. \tag{4}$$

The necking principle where the end radii being locked and the resulting deformation becoming nonlinear is the key to fine tuneable compliant structure of a CFT, this pitch variation with associated dimensions can be observed in Fig. 8, the pitch-radius coupling also follows directly from the helical development relation. Differentiation is given by equation (5),

$$\frac{dp}{dr} = -\frac{4\pi^2 r}{p}. \tag{5}$$

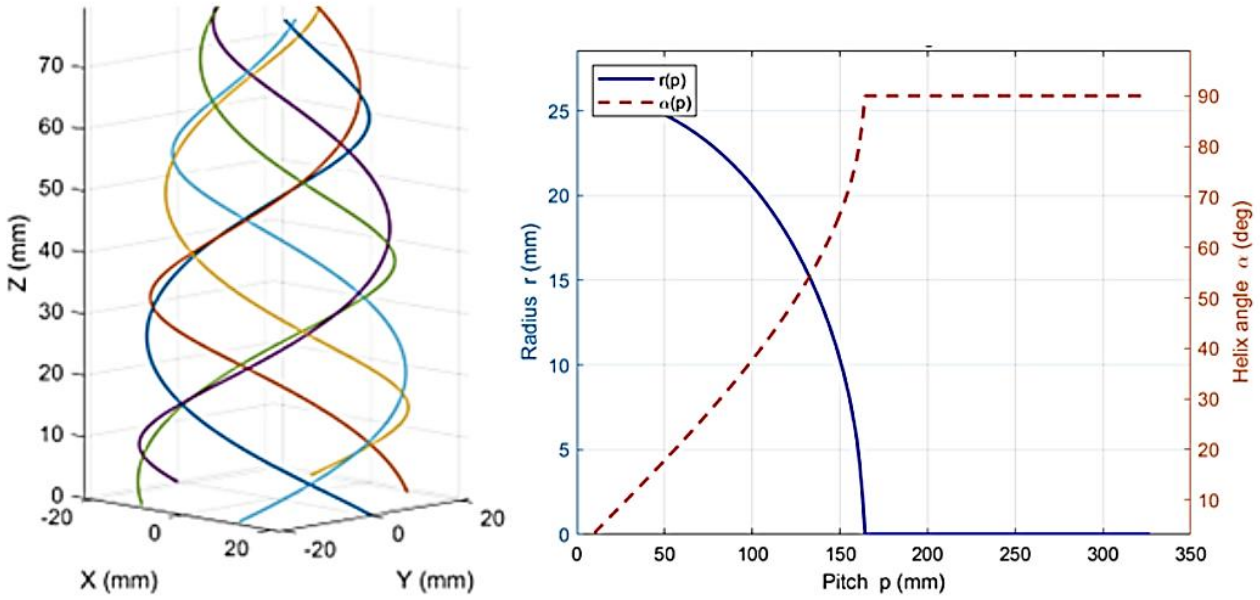


**Fig. 8.** Tuneable compliant structure of a CFT with pitch variation with related dimensions

The negative sign reflects the geometric fact that, for fixed strip length, increased axial pitch must be accompanied by reduced radius. This relation explains why axial extension and radial contraction are inseparable in the CFT mechanism.

For the fixed-end-radius case relevant to spoke applications, the CFT does not behave like a freely deforming toy finger trap. Instead, it develops a necking-type non-uniform profile. The mechanism-level response is represented through a bending-and-torsion energy framework in which the total stored energy is given by equation (6),

$$U = U_B + U_T = \sum \int_0^{L_i} (K_B \kappa^2 + K_T \tau^2)\, ds, \tag{6}$$

where $L_i$ is the segment length, $s$ is the arc length along the strip, $\kappa$ is the local curvature, $\tau$ is the local twist and the stiffness constants are given by equation (7),

$$K_B = E \cdot \frac{t^3 w}{12},\ K_T = G \cdot \frac{t^3 w}{3}, G = \frac{E}{2(1+v)}. \tag{7}$$

These expressions encode the thickness-cubed control, both bending stiffness $K_B$ and torsional stiffness $K_T$ scale with $t^3$, which is why thickness dominates stiffness tuning of the lattice segments. The local curvature and twist for a helix on a cylinder are given by equation (8),

$$\kappa = \frac{cos^2 \alpha_i}{r}, \tau = \frac{(\cos \alpha_i \cdot \sin \alpha_i)}{r} \tag{8}$$

and the axial force is obtained from the energy gradient as expressed in equation (9),

$$W = \int_0^{\Delta p} F dp = U(\Delta p), F(\Delta p) = \frac{dU(\Delta p)}{d(\Delta p)}, \tag{9}$$

where $\Delta p$ is the change in pitch or an equivalent axial deformation parameter. Because $U\Delta p$ is nonlinear through geometric coupling, the resulting force-displacement curve is nonlinear and treating the stiffness as either a tangent stiffness we get the axial stiffness, equation (10),

$$K_{ax} = \frac{dF}{dp}. \tag{10}$$

This energy-based logic is the mechanism foundation carried into the present hybrid spoke model. This demonstrates the impact of thickness on the stiffness of a CFT structure, which is controlled by its geometric properties rather than just the material properties alone.

### 2.3. Hybrid Coaxial Spoke Architecture

In order to preserve the compliant nature while gaining the ability to provide structural stability to the spoke, full-length CFT design transitions into a partially compliant with regionally deforming hybrid architecture. The hybrid implementation is to utilise compliant property of the CFT paired with stable elements paired in series configuration to achieve additional structural support.

The concept developed here is a coaxial structure with two elements, each with a CFT section paired in series configuration with a hollow tube, both are then connected in parallel configuration, where the ends are connected by base plates on both ends. The individual elements have CFT sections on opposite ends with respect to each other, in order to have independent activation of compliance for both elements triggered by the load applied on the connecting plate, as shown in Fig. 9. Given the requirement of pretension, the design is modelled to introduce geometric pretension, the spoke is designed to be shorter than total axial length required between the hub and the rim, which induces tension in the structure, this stretched installed state also adds to the stiffness of the structure due to the nonlinearly deforming CFT sections, resulting in higher radial load for further deformation.

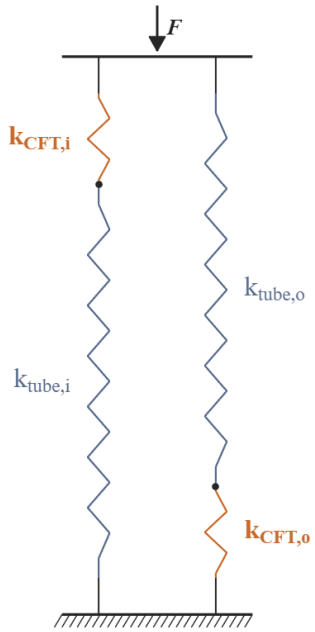


**Fig. 9.** Load application

This hybrid concepts allows control over compliance range, by controlling the geometric configuration of the CFT structure and the effective length of the CFT section in the overall element of the spoke. This delivers the nonlinear deformation while the coaxial tube provides the support which can also be tuned with changes in wall thickness and internal and external element diameters resulting in changes to installed-state support, alignment and buckling resistance.

## 2.4. Performance Targets and Fixed Wheel Level Assumptions

The hybrid spoke design is evaluated based on its performance under defined conditions and functional requirements. Primarily the concept spoke design is expected to provide a compliance resulting in overall hub deflection of 10 mm under the load case of 80 kg bicycle-rider system, while maintaining structural stability, avoiding permanent deformation and preserving the wheel's overall structural integrity.

The breakdown of the load case and its impact in the MATLAB screening process can be described by first splitting the load share between two wheels, 450 N with a 60 – 40 load share and a safety factor of 1.5 making the net resulting force under service conditions of 675 N. Targeting a spoke count under 28, derived by investigation of different CFT configurations in a range of 20 – 40 spoke count specifically under multiples of four which is the normal distribution of the contact forces as described in previous researches. The maximum static service-state hub deflection was limited to 2.5 mm as a rim protection criterion, the minimum branch buckling safety factor was set to 2.

**Table 3.** Summary of the acceptable values

| Parameter | Symbol | Value used | Purpose |
|---|---|---|---|
| **Functional hub-deflection target** | $\delta_{hub\ impact\ target}$ | ≥ 10 mm | Required impact-state hub travel |
| **Bicycle+rider design context** | — | 80 kg equivalent | Target application context |
| **Service design load** | $F_{wheel\ load}$ | 450 N | Baseline wheel-level service load |
| **Service safety factor** | SF | 1.5 | Conservative service screening |
| **Screened service load** | $F_{service}$ | 675 N | Effective service load |
| **Service radial gain factor** | $g_{service}$ | 0.90 | Converts spoke displacement to hub displacement |
| **Impact radial gain factor** | $g_{impact}$ | 1.00 | Converts spoke displacement to hub displacement |
| **Maximum static service hub deflection** | $\delta_{hub\ service\ max}$ | 2.50 mm | Rim-protection criterion |
| **Target wheel spoke count** | $n_{wheel\ target}$ | 28 | Maximum acceptable spoke count |
| **Spoke-count search range** | $n_{sweep}$ | 20–40, step 4 | Wheel feasibility search |
| **Minimum branch buckling safety factor** | $SF_{buckling\ min}$ | 2.0 | Stability requirement |
| **Maximum installed pretension per spoke** | $F_{pre\ max}$ | 120 N | Upper installed-force limit |
| **Minimum service-force threshold** | $F_{\min service}$ | 5 N | Slack-avoidance threshold |

Lastly the spoke is expected to provide impact-state hub radial deflection of 10 mm, a complete summary of the acceptable values used for the screening workflow and target list can be observed in Table 3.

## 2.5. Parametric Design Space and Array of Geometric Profiles

The hybrid spoke evaluation is conducted by treating them as groups of possible designs rather than individual geometries. The compliance aspect of the CFT section is controlled by the geometric variables, initial $H_0$, branch strap width, strip thickness and the turn count. This provides the control

over the compliance nature; further screening is enhanced by installation stretch and the material assigned to the supporting tube and the CFT section. This workflow is built on the foundational results established in the previous research, clearly demonstrating the impact of geometric parameters on the nonlinear behaviour, while the tube provides the missing support element, lacking in the previous design iteration. This is also to ensure the load-based activation of the CFT section of the spoke is an unbiased split among the two branches.

The parameters being investigated constitute the complete sample space for the screening process; the total number of variants swept is derived by equation (11).

$$N_{profiles} = H_0 \, x \, w_{outer} \, x \, w_{inner} \, x \, t \, x \, N \, x \, \Delta L_{install} \, x \, M_{tube} \, x \, M_{strip} \quad (11)$$

$$N_{profiles} = 6 \text{ x } 7 \text{ x } 5 \text{ x } 1 \text{ x } 5 \text{ x } 7 \text{ x } 2 \text{ x } 2 = 29.400.$$

The equation (11) has variables of $H_0$ – the length of the CFT section, $w_{outer}$ – outer branch widths, $w_{inner}$ – inner branch widths, $t$ – strip thickness, $N$ – turn count, $\Delta L_{install}$ – installation stretch, $M_{tube}$ – tube material, $M_{strip}$ – strip material, these boundary parameters result in a total of 29.400 profiles being screened, a summary of the parameters and their respective count can be found in Table 4.

**Table 4.** Summary of parameters

| Variable title | Symbol | Value considered | Values used in sweep |
|---|---|---|---|
| **Initial CFT height** | $H_0$ | 6 | 42, 48, 54, 60, 66, 72 mm |
| **Outer branch strip width** | $w_{outer}$ | 7 | 2, 3, 4, 5, 6, 7, 8 mm |
| **Inner branch strip width** | $w_{inner}$ | 5 | 1.5, 2.5, 3.5, 4.5, 5.5 mm |
| **Strip thickness** | $t$ | 1 | 0.8 mm |
| **Turn count** | $N$ | 5 | 1.0, 1.5, 2.0, 2.5, 3.0 |
| **Installation stretch** | $\Delta L_{install}$ | 7 | 6, 8, 10, 12, 14, 16, 18 mm |
| **Tube material** | $M_{tube}$ | 2 | PLA, CFRP |
| **Strip material** | $M_{strip}$ | 2 | PLA, CFRP |

The purpose of this sweep is to selectively shortlist the combinatorics of profiles that remain mechanically meaningful once the geometric, structural and wheel level constraints are imposed.

## 2.6. Installed State Design and Geometric Pretension Logic

The working principle of a standard bicycle spoke is tension; the preloaded installed state results in a prestressed wheel vital for the structural integrity. It is a prerequisite for the alternative hybrid spoke to be evaluated in the pretensioned state, not a free geometry. Instead, the design incorporates an installed-state bias by making the free branch lengths shorter than the installed hub-to-rim span. Once installed, the spoke is therefore stretched into an elastically biased state before any external service or impact load is applied.

If $L_{\text{free,outer}}$ and $L_{\text{free,inner}}$ are the free lengths of the outer and inner branches and $\Delta L_{\text{install}}$ is the imposed installation stretch, the common installed reference length is given by equation (12):

$$L_{install} = \frac{L_{free,outer} + L_{free,inner}}{2} + \Delta L_{install}. \quad (12)$$

The pre-extension of each branch relative to its own free state is then given by equations (13) and (14):

$$\Delta L_{pre,outer} = L_{install} - L_{free,outer}, \quad (13)$$

$$\Delta L_{pre,inner} = L_{install} - L_{free,inner}. \quad (14)$$

After installation, the spoke response is evaluated using a common displacement variable $u$, representing additional motion measured from the installed state. Thus, the installed condition is taken as $u = 0$, from which service and impact displacements are measured consistently.

In a linearized conceptual form, installed-state bias may be interpreted through equation (15):

$$F_0 = k\Delta L_{inst}, \; k = \frac{EA}{L_0}. \quad (15)$$

Although the actual hybrid response is nonlinear, the installed force is recovered from the branch backbones rather than imposed from a linear spring law. This ensures that the geometric pretension is sufficiently induced to support the structure but at the same time doesn't solely operate using the tensioned wheel principle conventional spoke use.

The screen used a minimum service pretension of 5 N. This is not the final pretension of an actual bicycle wheel. It is a conservative slack-avoidance value below which a profile is not considered to be providing appreciable tension in the low order service screen. Structural adequacy is therefore not judged by this threshold alone, but by its interaction with service deflection, spoke count, and buckling reserve.

## 2.7. Reduced Order Hybrid Spoke Model

The reduced-order hybrid model is the principal design-screening tool. Its purpose is not to reproduce every local contact or full-wheel effect in detail, but to evaluate a very large design space in a mechanically interpretable and computationally efficient way so that only meaningful profiles proceed to embodiment and simulation.

Each hybrid spoke is represented by two branches: an outer branch and an inner branch. Within each branch, the CFT-derived compliant region and the coaxial straight tube are treated as elements acting in series. At the full spoke level, the outer and inner branches act in parallel.

– ***Tube representation***

A coaxial straight structural approach is used to enhance the design, this is to address the lack of axial stability and buckling issue experienced in full length CFT compliant spoke, this coaxial straight tube is represented by its annular cross-section and axial stiffness. The tube cross-sectional area is given by equation (16):

$$A = \frac{\pi}{4}(OD^2 - ID^2) \quad (16)$$

and the corresponding axial stiffness is given by equation (17):

$$k_{tube} = \frac{EA}{L}, \quad (17)$$

where *OD* and *ID* are outer and inner tube diameters, *E* is the Young ‘s modulus of the tube material, and *L* is the effective tube length.

This expression is used because the main purpose of the central tube is to provide structural stabilisation and not the main source of compliance. Its function in the hybrid spoke is to distribute the axial loading efficiently, provide direction stability and increase buckling resistance. The linear structural component is coupled with the nonlinear CFT response, and the resulting tube is a good stability element, which is screened through the MATLAB framework.

– ***Common displacement variable***

After installation, the spoke response is expressed in terms of a single displacement variable u, which is the displacement from the installation state. The displacement of the outer and inner branches is therefore equations (18) and (19):

$$x_{total,outer} = \Delta L_{pre,outer} + u\ , \tag{18}$$

$$x_{total,inner} = \Delta L_{pre,inner} + u. \tag{19}$$

This is useful because it enables a common displacement variable to be used for the installation, operational, and impact cases. Rather than solving the problem for each state, the MATLAB code evaluates the spoke over a range of displacement about the installed state. This enables the pretension, stiffness, lock onset, and wheel performance to be extracted from a common response.

– ***Series compatibility between the tube and the CFT branch***

Within each branch, the compliant CFT section and the coaxial tube are treated as elements acting in series. The total branch extension is therefore the sum of CFT deformation and tube deformation given by equation (20):

$$x_{total} = x_{CFT} + x_{tube}. \tag{20}$$

With the axial deformation of tube is represented by equation (21):

$$x_{tube} = \frac{F}{k_{tube}}, \tag{21}$$

where *F* is the branch force. The unknown CFT deformation is then determined by enforcing displacement compatibility through the residual expression given in equation (22):

$$g(x_{CFT}) = x_{CFT} + \frac{F_{CFT}(x_{CFT})}{k_{tube}} - x_{total} = 0. \tag{22}$$

This equation is one of the core equations of the reduced-order model. It ensures that the nonlinear deformation of the CFT and the axial deformation of the tube remain mechanically consistent for any imposed branch displacement. The branch response is therefore not prescribed directly, but obtained from the interaction of a nonlinear compliant mechanism and a linear structural support member.

– ***Series stiffness of each branch***

Once the CFT branch tangent stiffness $K_{\mathrm{CFT}}$ is known, the effective branch stiffness is obtained by a series combination given by equation (23):

$$K_{series} = \left(\frac{1}{k_{tube}} + \frac{1}{K_{CFT}}\right)^{-1}. \quad (23)$$

This expression is important, because it defines the architectural design space of the hybrid. The tube provides stiffness and stability to the structure and the CFT provides compliance. So, the series connection defines the effective stiffness of each branch and the amount of deformation that is "absorbed" by the compliant mechanism and the amount that is absorbed by the axial deformation of the tube.

– ***Parallel branch assembly***

The total spoke force and stiffness are therefore obtained by summing the branch contributions given which act together as parallel components consisting of inner and outer branches, by equation (24) and (25):

$$F_{total}(u) = F_{outer}(u) + F_{inner}(u), \quad (24)$$

$$K_{total}(u) = K_{outer}(u) + K_{inner}(u). \quad (25)$$

Installed-state quantities are evaluated at $u = 0$, giving equation (26) and (27),

$$F_{pre,total} = F_{total}(0), \quad (26)$$

$$K_{pre,total} = K_{total}(0), \quad (27)$$

which give installed force, installed stiffness, branch force split, installed strain and motion reserve to lock-up. The installed branch force fraction is in equation (28) and (29),

$$\varphi_{outer,install} = \frac{F_{pre,outer}}{F_{pre,total}}, \quad (28)$$

$$\varphi_{inner,install} = \frac{F_{pre,inner}}{F_{pre,total}}. \quad (29)$$

These are important to the rejection algorithm because they indicate a significant preloaded spoke rather than a slack or single branch compliant spoke.

– ***Contact, friction and lock up treatment***

As the CFT deforms, strip-strip contact is established and affects the axial response, especially at lock-up. The screening algorithm therefore includes a measure of contact fraction as a measure of proximity to geometric lock-up. But the approach does not claim to be a first-principles friction-resolved contact model. Instead, the branch response is still geometry- and energy-driven and contact and friction are second-order effects, based on past experiments and observations.

For each branch, the first positive displacement at which the contact fraction reaches the lock threshold is taken as the branch lock displacement given by equation (30),

$$u_{lock} = \min\{u \geq 0 : c_f(u) \geq c_{f,lock}\}. \quad (30)$$

The first system lock displacement is then defined as the earlier of the two branch lock onsets, given by equation (31),

$$u_{first\ lock} = \min\left(u_{lock,outer}, u_{lock,inner}\right). \quad (31)$$

Since the installed state is defined as $u = 0$, the remaining lock margin is equal to $u_{first\ lock}$.

## 2.8. Wheel Level Service, Impact and Spoke count Screening

The reduced-order model is used not only to generate local force-displacement curves but also to map spoke behaviour into wheel-relevant acceptance criteria. Because a full wheel FEA sweep of all profiles would be impractical, the MATLAB framework uses simplified but explicit load-sharing rules for service and impact states.

At service state, the incremental force carried by one spoke is approximated as shown in equation (32),

$$\Delta F_{spoke} = \frac{F_{local\ load}}{n_{eff}}, \quad (32)$$

where $n_{eff}$ is the effective number of spokes sharing the load.

A first order hub deflection estimate can be written using equation (33),

$$\delta_{hub,service} = g_{service} \frac{\Delta F_{spoke}}{K_{pre,total}}, \quad (33)$$

where $g_{service}$ is the service radial gain factor.

Because the spoke response is nonlinear, the screening framework uses a more consistent form based on inversion of the incremental force-displacement response given by equation (34),

$$\delta_{hub,service} = g_{service} u_{service}. \quad (34)$$

The service state criteria are then given by equation (35 – 37),

$$F_{pre,total} - \Delta F_{service,spoke} \geq F_{min,service}, \quad (35)$$

$$\delta_{hub,service} \leq 2.5\ \text{mm}, \quad (36)$$

$$SF_{buckling} \geq 2.0. \quad (37)$$

The minimum spoke count required for service feasibility is determined by searching profiles wheel counts from 20 to 40 in steps of four and identifying the smallest count that satisfies the service screen. A profile is accepted only if it satisfies equation (38),

$$N_{wheel,min} \leq 28. \quad (38)$$

Thus, spoke count is not prescribed geometrically in advance, but found through service feasibility screening.

At impact state, a corresponding force share approximation is used given by equation (39),

$$\Delta F_{impact} = \frac{F_{impact,local}}{n_{eff}}. \quad (39)$$

The nonlinear displacement being $u_{impact}$, hub level deflection is given by equation (40),

$$\delta_{hub,impact} = g_{impact} u_{impact}. \quad (40)$$

The impact success criterion is given by equation (41),

$$\delta_{hub,impact} \geq 10 \text{ mm}. \quad (41)$$

Together, these service and impact criteria ensure that a profile is not accepted simply because it deforms. It must deform while preserving service support, buckling reserve, and feasible wheel spoke count.

### 2.9. Buckling Treatment and Profile Rejection Logic

The purpose of the hybrid stabilizing span is not only to support installed-state force, but also to improve resistance to instability. For each annular tube-supported branch, the second moment of area is given by equation (42),

$$I = \frac{\pi}{64} (OD^4 - ID^4). \quad (42)$$

The Euler type branch buckling load used in the screening is given by equation (43),

$$P_{cr} = K_{buckling} \frac{EI\pi^2}{L^2}, \quad (43)$$

where $K_{buckling}$ is used as a buckling coefficient in the model.

The branch buckling safety factor is then given by equation (44),

$$SF_{buckling} = \frac{P_{cr}}{F_{ref}}. \quad (44)$$

This notation should be stated clearly so that it is not confused with the conventional effective-length-factor notation of classical Euler buckling.

Profile rejection was hierarchical rather than based on a single objective. This was necessary because a design that is highly compliant is not automatically viable. It must also be geometrically admissible, support-capable, not prelocked in installation, sufficiently balanced between branches, and able to satisfy wheel-level requirements.

The main rejection stages were:

- geometric admissibility – remove profiles violating CFT geometry rules;
- installed state viability – require sufficient installed support, adequate lock margin, acceptable installed strain, and adequate branch participation;
- service state feasibility – require service retention, acceptable static hub deflection and feasible spoke count;
- buckling safety – require branch buckling safety factor above the prescribed threshold;
- impact performance – require at least 10 mm hub radial deflection.

Table 5 has the threshold values listed used for screening purpose.

**Table 5**. Values used for screening purpose

| Screening stage | Criterion | Threshold | Interpretation |
|---|---|---|---|
| **Geometry admissibility** | CFT geometry validity | Must satisfy geometric feasibility rules | Rejects impossible woven configurations |
| **Installed-state support** | Minimum installed service-support force | $F_{pre,total} > 5$ N | Rejects effectively slack profiles |
| **Installed-state lock fraction** | Installed contact/lock level | $\leq 0.15$ | Profile must not begin too close to lock-up |
| **First-lock margin** | First positive lock displacement | $\geq 1$ mm | Profile must retain usable motion |
| **Installed-state strain** | Maximum installed strain | $\leq 0.06$ | Prevents excessive initial deformation |
| **Branch-force participation** | Minimum branch force fraction | $\min(\varphi_{outer}, \varphi_{inner}) \geq 0.05$ | Prevents one branch becoming irrelevant |
| **Service-state retention** | Support maintained under service increment | $F_{pre,total} - \Delta F_{service,\ spoke} \geq F_{min,\ service}$ | Profile remains tensile/support-capable |
| **Static service hub deflection** | Rim-protection criterion | $\delta_{hub\ service} \leq 2.5\ mm$ | Prevents excessive service displacement |
| **Installed pretension upper limit** | Maximum installed force per spoke | $\leq 120$ N | Rejects overly highly tensioned profiles |
| **Buckling safety** | Minimum branch buckling safety factor | $SF_{buckling} \geq 2.0$ | Requires sufficient stability |
| **Wheel spoke-count feasibility** | Minimum required wheel spoke count | $n_{wheel,\ rim}$ | Profile supports feasible wheel configuration |
| **Impact-state success** | Hub deflection target | $\delta_{hub,impact} \geq 10\ mm$ | Profile satisfies main objective |

## 2.10. CAD Modelling

Only profiles surviving reduced-order screening were carried into CAD. This stage is important because reduced-order modelling alone cannot capture section transitions, interface embodiment, packaging, and the physical coherence of the final part. The purpose of CAD was therefore not to invent the concept, but to determine whether a mathematically viable profile could be modelled as a realistic spoke-like component.

The final modelled geometry consists of a long tube-supported span, a localized CFT-derived compliant region near one end, and a circular-disc housing intended to accommodate inserts and fastening. The total geometry is approximately 265 mm long, consistent with the intended wheel packaging as shown in figure xx. The CAD model therefore acts as the bridge between the reduced-order parameter set and a real buildable component definition.

## 2.11. Static Simulation Setup

Static simulation was carried out in SOLIDWORKS Simulation as a later-stage component-level assessment of the modelled hybrid spoke. The purpose of this stage was not to reproduce complete wheel behaviour and not to serve as final product validation It was, however, used to determine if the shortlisted geometry was mechanically viable when implemented as a 3D part, and to identify possible deformation and stress concentration.

The problem was modelled as a static solid mesh analysis. One end of the spoke was fixed and a 200 N load was applied to the other end. It was assigned a linear elastic isotropic material, Thornel Mat VMA, with $E$=70 GPa, Poisson's ratio 0.30 and density 1600 kg/m$^3$. Global contact was set to be surface-to-surface but interaction between strips was defined as local contact with friction coefficient of 0.15 and large-displacements were turned off, as the goal was a first-order embodied structural analysis, not a full contact analysis.

The mesh was generated as a blended curvature-based solid mesh containing 45.296 nodes and 21.258 elements, with a maximum element size of 7.37 mm and a minimum element size of 0.369 mm. The outputs of interest were resultant displacement, von Mises stress, and the location of dominant deformation and stress concentration. These outputs are interpreted later in the Chapter 3.

## 2.12. Prototype Fabrication and Experimental Procedures

Experimental work is used as physical grounding rather than as complete production-level validation. Two experimental contexts are relevant, the preceding full-length CFT proof-of-concept stage and the later hybrid specimen stage. In both cases, additive manufacturing was used to produce repeatable geometries for mechanism and architecture evaluation.

For the earlier full-length CFT prototype, the purpose of fabrication was to test whether the CFT mechanism produced the expected nonlinear behaviour under cyclic tensile and compressive loading. For the hybrid specimen, fabrication also served to evaluate whether the combined architecture could be produced and repeatedly loaded in a physically meaningful way. Because internal CFT regions were difficult to access and clean after printing, standard support strategies were not always suitable. In the hybrid case, customized support logic was adopted so that the internal compliant region could be printed while avoiding support configurations that could not later be removed cleanly. This fabrication strategy is important because manufacturability was itself part of the practical architectural assessment.

Where needed, slicing software views may be shown to document the fabrication strategy, especially for the hybrid configuration where internal access constraints influenced support design. These images should be used in Methodology only to explain how the part was made, not to discuss the outcomes of testing. Detailed slicing screenshots are better suited to an appendix unless they directly support a unique fabrication argument in the main text.

Mechanical testing was used to evaluate the force-displacement behaviour of the printed structures under controlled loading. For the full-length concept, UTM-based testing established the mechanism-level response under cyclic loading. For the hybrid concept, cyclic testing was used to assess repeated loading behaviour and to provide physical evidence of branch participation and architectural durability. Where post-test slotting or opening of the hybrid specimen was used to reveal internal damage or hidden branch failure, that procedure should be described here as part of the test inspection method, while the actual observed failure pattern should be reserved for the Chapter 3.

## 3. Results

### 3.1. Results Carried Forward from Full-Length CFT

The work in this thesis extends the previous full-length Chinese finger trap (CFT) spoke. These are backdrop results to be continued, rather than the primary new results of this work. They are employed to justify the further use of the CFT mechanism, and the hybridisation into a coaxial mechanism.

The previous study demonstrated that the CFT geometry can be defined by fixed wheel-interface constraints, strip geometry, turn count and material. The long-length CFT had fixed interface span (about 275 mm), fixed end constraint diameter (24 mm), six strips in three pairs, and design variables for the strip width, strip thickness, turn count and material as shown in Fig. 10. The Python screening used the critical-width feasibility condition to eliminate geometrically-infeasible cases. This demonstrated the design space of the CFT is not open: some strip widths and turn counts are geometrically-infeasible because the woven geometry is too tight or not weavable.

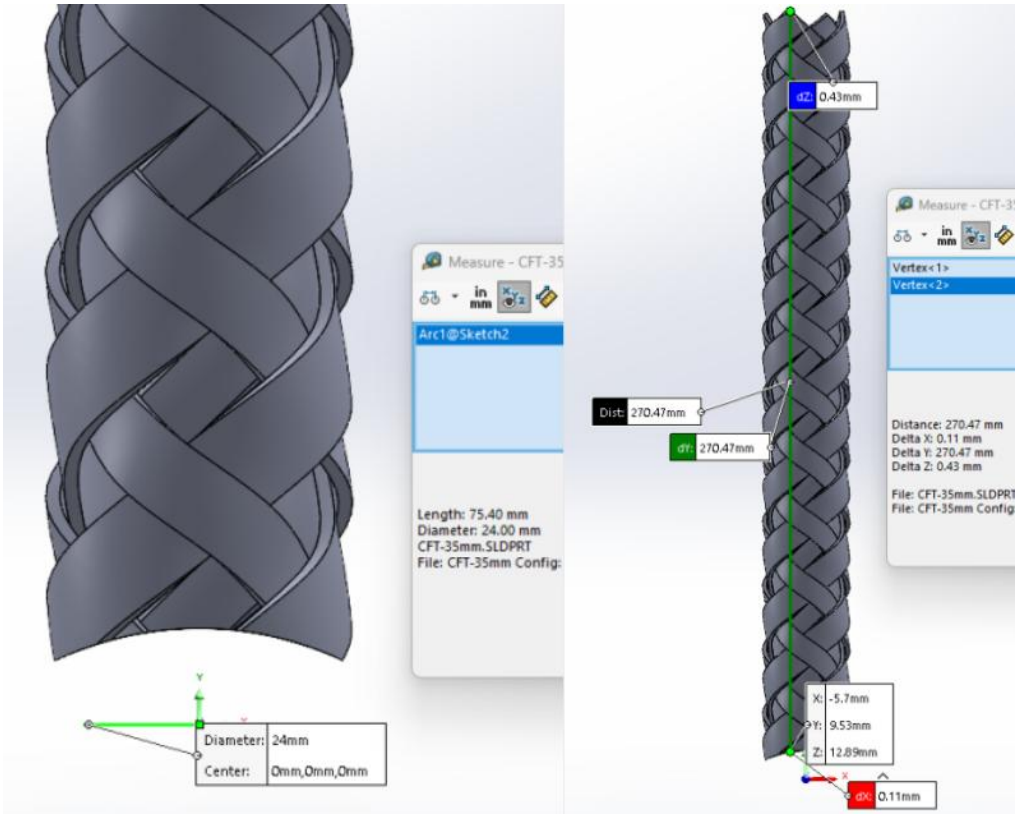


**Fig. 10.** Design of strip

The MATLAB nonlinear model indicated that the full-length CFT could be a nonlinear spring. The CFT was not a linear spring for a given end radius. It was a softening spring that stiffened towards geometric lock-up. This was significant as it showed that the CFT mechanism could, in theory, be used to provide controlled compliance, rather than material softening. The research provided a wheel-level estimate of 11 mm of hub deflection for the chosen configuration, implying that the CFT mechanism could provide the required order of magnitude of hub deflection.

The full-length CFT was also compared with two loopwheel-type references using a static wheel-level simulation. Under the given comparison conditions, the CFT wheel concept generated about

9 mm of hub deflection, as seen in Fig. 11 while the two loopwheel-type references generated about 3.3 mm and 5.9 mm, respectively. This indicated that the CFT mechanism was comparable with other mechanisms that produce compliance and can be expected to produce more hub deflection than the two references in the comparative simulation test.

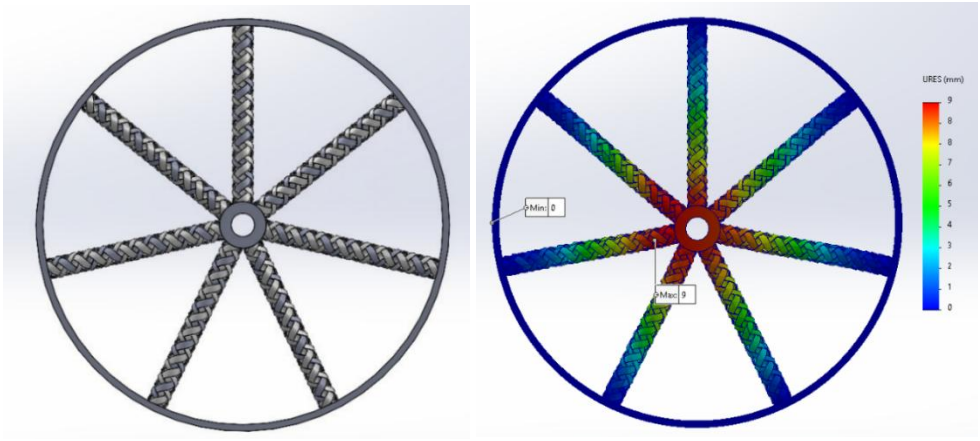


**Fig. 11.** Concept of CFT wheel and its static simulations


**Fig. 12.** Setup of experiments in UTM

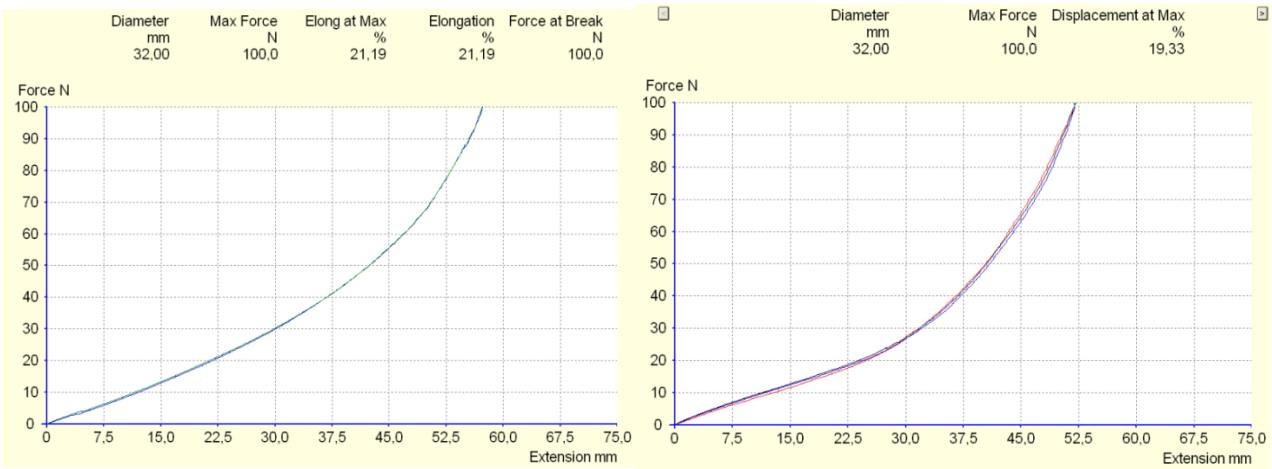


**Fig. 13.** Test results of tension and compression

The test was the most physical test. A full-scale specimen of PLA CFT was fabricated and tested in tension and compression in UTM, setup shown in Fig. 12. This demonstrated initial soft behaviour, followed by stiffening and locking up at 37.5 mm, as seen in Fig. 13. This demonstrated the nonlinearity was not only theoretical, but real.

But the full-length CFT test also showed the major weakness in this thesis. The mechanism was right but the architecture was undisciplined as a whole spoke. The full-length spoke was compliant along the whole length, and so was unstable, non-uniformly deformed and buckled, as seen in Fig. 14. So, the full-length CFT was not developed as a final spoke. It was developed as a mechanism for the current hybrid coaxial spoke, where the CFT is isolated as a compliant substructure and the rest of the spoke is stiffened. Overall summary of the preceding research can be understood from Table 6.

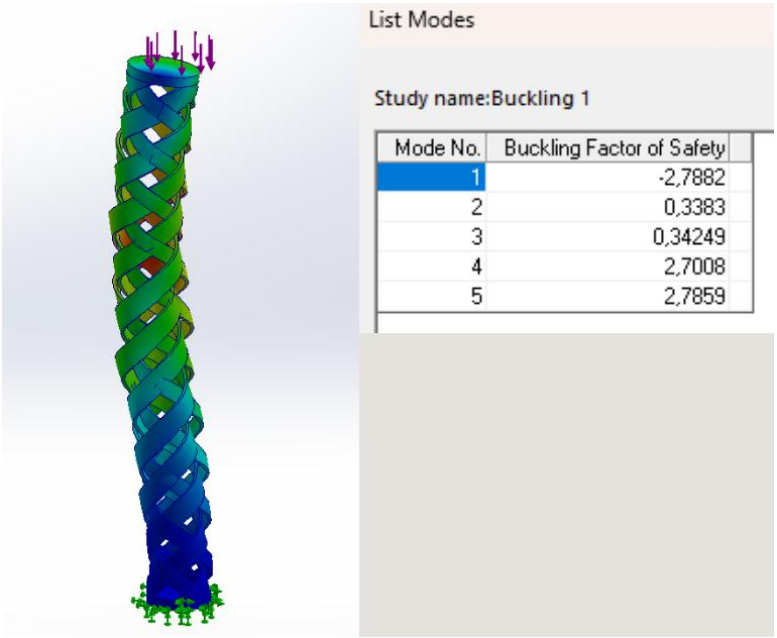


**Fig. 14.** Results of non-uniformly deformed and buckled spoke

**Table 6.** Summary of research

| Result category | Main finding | Role |
|---|---|---|
| **Geometric screening** | Critical-width screening removed inadmissible CFT geometries | Provided the geometric admissibility logic |
| **MATLAB nonlinear prediction** | Nonlinear force–deflection behaviour and progressive stiffening were observed | Confirmed the CFT as a useful compliant mechanism |
| **Wheel-level estimate** | Approximately 11 mm hub deflection predicted | Showed that the mechanism could reach the target order of travel |
| **Comparative wheel simulation** | CFT wheel concept produced ~9 mm hub deflection compared with ~3.3 mm and ~5.9 mm for two Loopwheel-type references | Supported the CFT as a promising compliance mechanism |
| **UTM cyclic testing** | Progressive stiffening and lock-up after ~37.5 mm of motion | Physically validated the mechanism behaviour |
| **Main limitation** | Full-length compliance caused instability and buckling vulnerability | Motivated transition to hybrid architecture |

### 3.2. Preliminary Hybrid Specimen and Motivation for Screening Improvements

Following the problems with the full-length CFT, a hybrid CFT was designed and built. This was the first attempt to preserve the desirable nonlinear behaviour of the CFT and enhance the structural performance by using a hybrid design. The hybrid had local CFT compliant branches and a straight branch, in place of the full-length CFT, as displayed in Fig. 15.

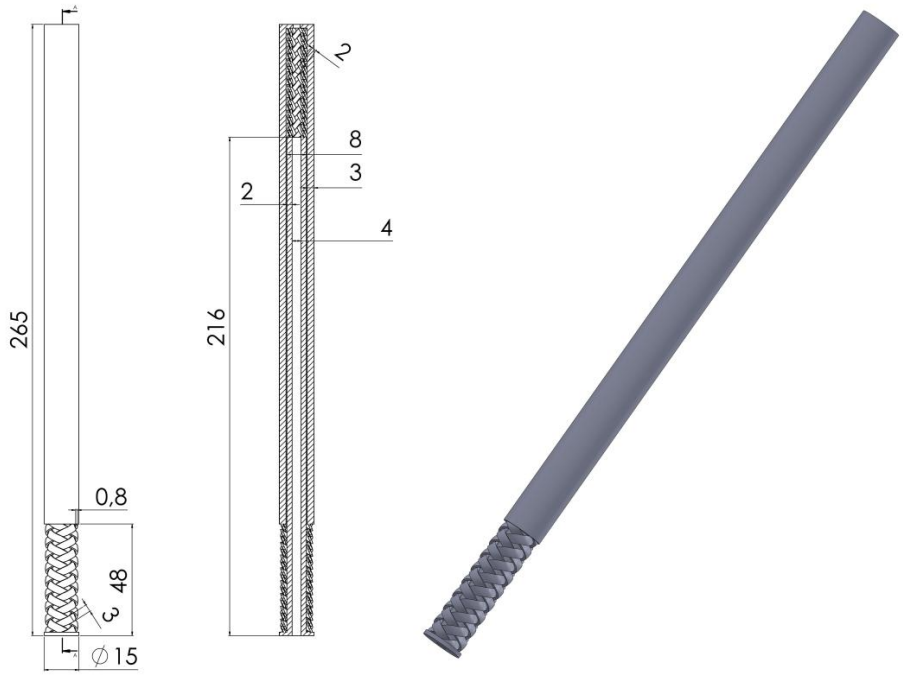


**Fig. 15.** Hybrid CFT dimensions and view

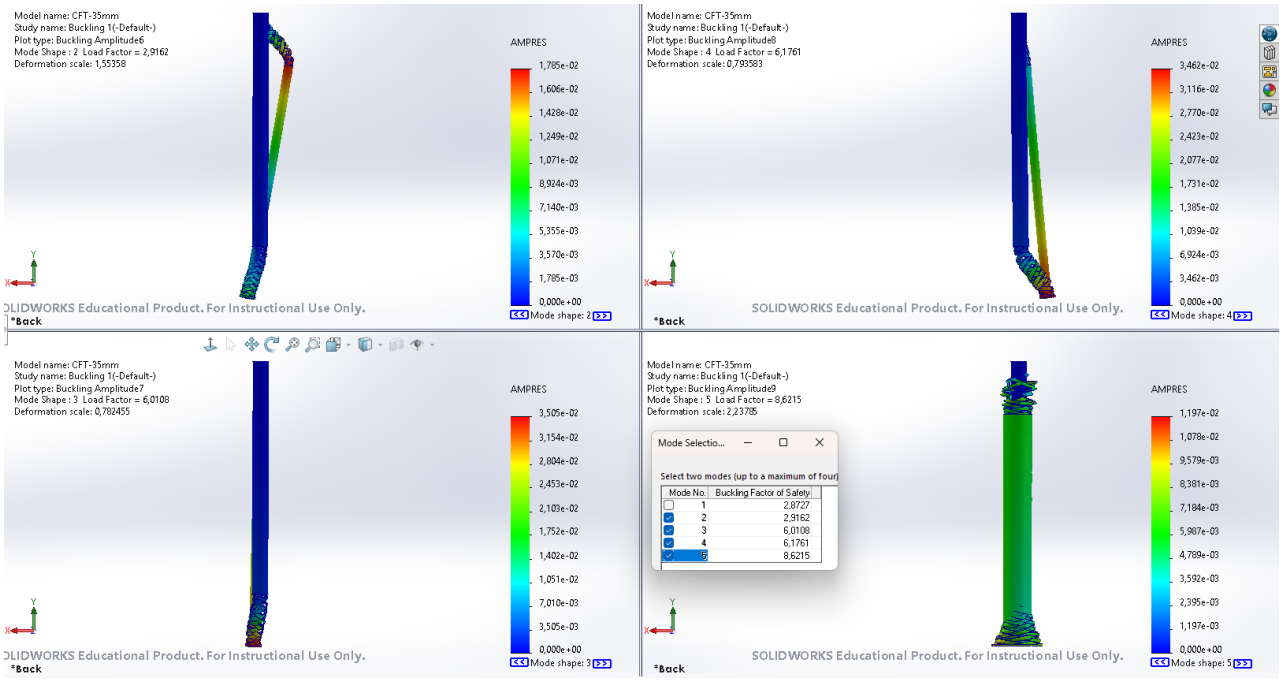


**Fig. 16.** Test results of feasibility verification

The first hybrid was cyclically tested, to verify the feasibility of the concept, and the engagement of the compliant branches. It was shown to be physically and mechanically feasible, with improvements in the buckling safety factors as well, seen Fig. 16, but also that there was a problem with branch-load sharing. The hybrid was then cut to check the inner CFTs. This indicated that the inner CFT had cracked before the outer CFT had been mobilised.


**Fig. 17.** The setup for experiment of cyclic testing

The setup for the simulation was maintained under the same static simulation conditions to keep the same baseline for correctly mapping the improvements, for experiment of cyclic testing the setup can be seen in Fig. 17.

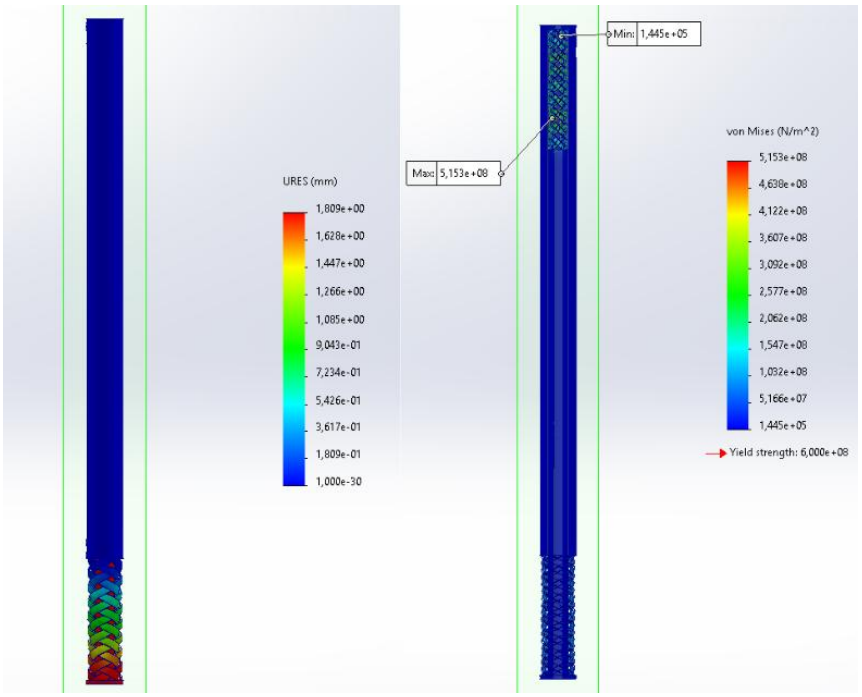


**Fig. 18.** Results of specimen's flexibility

This was significant as it meant the hybrid structure could not be assessed purely on the displacement or stiffness. The specimen could be flexible but a part of the branch failed, as observed in Fig. 18 the simulation results where the internal CFT section bears the maximum stress, and Fig. 19 the results of the experimental cyclic testing, with the damaged cross-section opened view. In the preliminary specimen the inner CFT was the first to enter the active deformation regime and was thus overloaded. The outer CFT did not have time to participate.

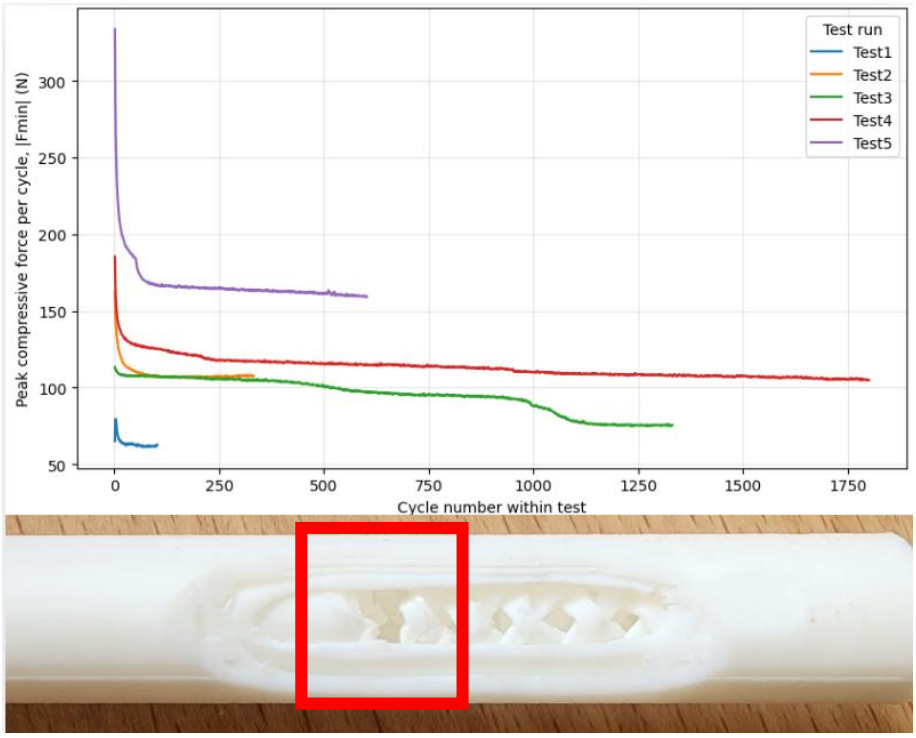


**Fig. 19.** Results of the experimental cyclic testing with the damaged cross-section opened view

This affected the MATLAB screening logic. The screening criteria were thus branch-force participation and load-balance, so that a design was not acceptable if one branch did not participate or the response was too flexible in one direction. So, the preliminary hybrid specimen was not a failed final design, but rather a test specimen that identified a criterion. The summary of the observations made in hybrid model simulation and testing, and their role in further development are observed in Table 7.

**Table 7.** The summary of simulation and testing results

| **Observation** | **Interpretation** | **Consequence for later screening** |
|---|---|---|
| Inner CFT fractured internally after cyclic testing | Inner branch activated earlier and carried excessive load | Branch-load balance became a required screening condition |
| Outer CFT was not fully active before inner damage | Parallel branches were not participating equally | Minimum branch-force participation criterion was added |
| Cyclic response showed real contact and damage effects | Reduced-order model required conservative filtering | Profile selection was based on support, lock margin, and branch participation, not displacement alone |
| Hybrid architecture remained manufacturable and testable | Concept was physically plausible but needed better tuning | Final profiles were selected through expanded MATLAB screening |

### 3.3. MATLAB Screening Output and Profile Reduction

The final low-order screening, in MATLAB, was then performed on a wide range of hybrid spokes after considering the lessons learned from the preliminary hybrid specimen. This process was not applied to identify the most flexible profile. Rather, the screening process was used to select profiles that meet the geometry, installed-state support, lock-margin, branch-participation, service-state, spoke-count, buckling and impact-response criteria.

29.400 profiles were screened. These were obtained by varying the CFT section length, outer branch width, inner branch width, strip thickness, turn count, installation stretch, tube material and strip material. The screening process was hierarchical. They were first checked for geometric feasibility. Then, for support in installed state, support in service state, feasibility of spoke count, buckling safety, and impact performance.

The screening reveals a small design space. Only four out of 29.400 designs have been found to be thesis-successful. This is one of the thesis' contributions because it shows the hybrid CFT spoke problem is very limited. It was not enough to have high hub travel. It also had to be supportable, not prematurely locking, branch-participating, have service-state deflections, be stable, and reach the impact hub-deflection target. Workflow and rejection process summarised in Table 8.

**Table 8.** Workflow and rejection process

| **Screening outcome** | **Number of profiles** |
|---|---|
| Total generated profiles | 29.400 |
| Geometry rejects | 4.676 |
| Installed/local-state rejects | 14.169 |
| Service-state failures | 8.054 |
| Target spoke-count failures | 1.689 |
| Impact-response failures | 808 |
| successful profiles | 4 |

The fact that the final shortlisted profiles were reduced from 29.400 to just four successful profiles confirms that the final profiles were not chosen at random. They passed a tough engineering test. This is important because the final profiles are a small region where compliance, support, lock margin, spoke-count feasibility and stability are all acceptable.

### 3.4. Shortlisted Geometric Profiles

The four successful MATLAB profiles were design IDs 7376, 7390, 12524, and 13224. The four profiles were clearly two distinct design families (Table 9).

Profiles 7376 and 7390 were from the 14 mm installation-stretch family. They had lower installed stiffness and greater lock margin and were compliance-oriented. Profiles 12524 and 13224 were from the 6 mm installation-stretch family. They had higher installed stiffness, lower service deflection and lower spoke count, and were support-oriented profiles.

This is important because the thesis' final solution is not a universal optimum. Rather, the screening process identified a trade-off between two equally valid design choices: compliance-oriented design (impact travel and compliance reserve) and support-oriented design (support and conservatism).

**Table 9.** Properties of profiles

| Profile ID | $H_0$ | $w_{outer}$ | $w_{inner}$ | $t$ | $N$ | $\Delta L_{install}$ | Tube material | Strip material | Family |
|---|---|---|---|---|---|---|---|---|---|
| 7376 | 48 mm | 5.0 mm | 3.5 mm | 0.8 mm | 2.5 | 14 mm | baseline tube | CFRP strip surrogate | Compliance -oriented |
| 7390 | 48 mm | 5.0 mm | 3.5 mm | 0.8 mm | 2.5 | 14 mm | CFRP tube | CFRP strip surrogate | Compliance -oriented |
| 12524 | 54 mm | 5.0 mm | 5.5 mm | 0.8 mm | 2.0 | 6 mm | baseline tube | CFRP strip surrogate | Support-oriented |
| 13224 | 54 mm | 6.0 mm | 5.5 mm | 0.8 mm | 2.0 | 6 mm | baseline tube | CFRP strip surrogate | Support-oriented |

The MATLAB visualiser output for profile 7376 was typical of the compliance family. The profile showed a wide displacement window before first lock and a nonlinear force response with a stiffening response at high deformations. The load-sharing response was also better than the preliminary experiment because the screening process ensured that profiles with very little branch participation were not selected.

### 3.5. Installed State Behaviour

The results for the installed state show the behaviour of the shortlisted profiles before they receive additional service or impact loads. This is necessary because a spoke-like element can't be evaluated in its free state. It needs to offer some installed support, but also allow for sufficient displacement before lock-up.

Profiles 7376 and 7390 had installed stiffnesses of 15.38 N/mm and 15.54 N/mm respectively. Their lock margin was 20.87 mm and 20.49 mm respectively. It shows that the 14 mm installation-stretch family had a significant deformation margin left after installation. With the force factor resulting in values of 44.51 N and 43.52 N respectively, as shown in Fig. 20.

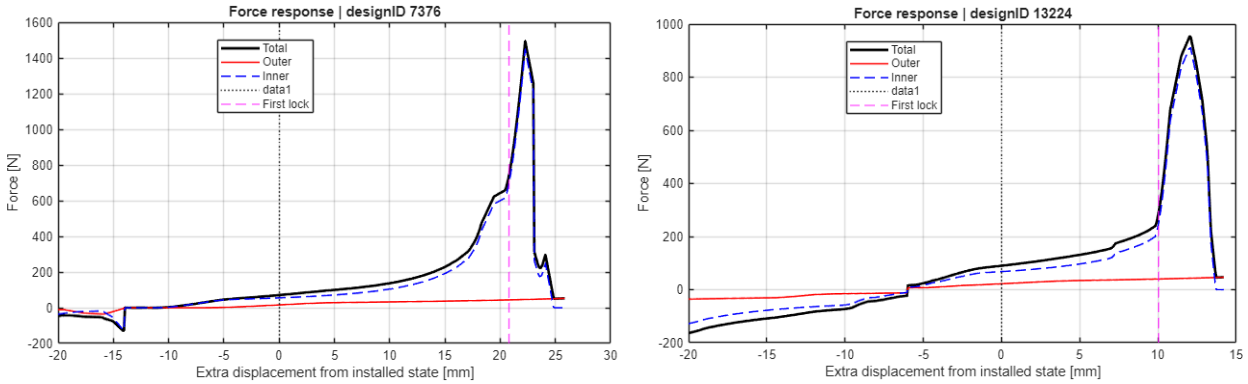


**Fig. 20.** Results of profiles behaviour

Profiles 12524 and 13224 had greater installed stiffnesses of approximately 29.41 N/mm and 30.01 N/mm respectively. Their lock margins were both approximately 10.21 mm. This implies that the 6 mm installation-stretch family was stiffer and support-oriented, but had less motion reserve.

**Table 10.** Properties of the installed spokes

| Profile ID | $F_{pre,total}$ | $K_{pre,total}$ | Lock margin | Installed-state interpretation |
|---|---|---|---|---|
| 7376 | 44.51 N | 15.38 N/mm | 20.87 mm | Lower stiffness, high motion reserve |
| 7390 | 44.86 N | 15.54 N/mm | 20.49 mm | Lower stiffness, high motion reserve |
| 12524 | 39.91 N | 29.41 N/mm | 10.21 mm | Higher stiffness, lower motion reserve |
| 13224 | 43.52 N | 30.01 N/mm | 10.21 mm | Higher stiffness, lower motion reserve |

The comparison of the installed spokes (Table 10) confirms the influence of installation stretch on the mechanical function of the spoke. The profiles with larger installation stretch retained more compliance after installation, whereas profiles with smaller installation stretch started the operating condition with greater stiffness and support. This finding confirms the later interpretation of 7376 as the "compliance" profile and 13224 as the "support" profile.

### 3.6. Service State Feasibility and Spoke Count Support

The results from the service state determine whether a profile can act as a wheel-relevant support member, in addition to a compliant mechanism. The design must provide support under service loading, be within the static hub-deflection limit and meet the spoke-count target.

Profiles 7376 and 7390 needed 28 spokes to pass the service screen (Table 11). Their service hub-deflections were around 1.36 mm and 1.34 mm respectively. These deflections were still below the adopted service limit, but greater than the support profiles. This confirms that the 14 mm installation-stretch family is more compliant, but needs the target number of spokes to be service feasible.

Profiles 12524 and 13224 only needed 20 spokes (Table 11). They had service hub deflections of approximately 0.97 mm and 0.95 mm respectively. This demonstrates the service-efficiency of the 6 mm installation-stretch family. The lowest service hub deflection of the four successful profiles was achieved by profile 13224, which is thus the best service-support profile.

**Table 11**. Results of profiles' hub-deflection limit and their the spoke-count

| Profile ID | Required spoke count | Service hub deflection | Service-state interpretation |
|---|---|---|---|
| 7376 | 28 | 1.36 mm | Pass; compliance-oriented but requires full target spoke count |
| 7390 | 28 | 1.34 mm | Pass; compliance-oriented but requires full target spoke count |
| 12524 | 20 | 0.97 mm | Pass; support-oriented |
| 13224 | 20 | 0.95 mm | Pass; strongest service-support profile |

The service-state results are important because they show that the more compliant profiles are not automatically the best spoke profiles. A spoke must preserve wheel support. From this perspective, 13224 is the most conservative service profile because it combines low service deflection with a lower required spoke count.

### 3.7. Impact Response Performance

The impact-response screen assesses the key functional goal of the thesis: to have at least 10 mm radial hub deflection in the impact-state condition. This target was met by all four shortlisted profiles, but with large differences between the two families.

The impact hub deflections of profiles 7376 and 7390 are around 14.54 mm and 14.39 mm respectively. These are more than 4 mm above the 10 mm target and demonstrate that the 14 mm installation-stretch family has a lot of compliance. These profiles are therefore the best choices if the primary goal is to maximise hub travel.

Profiles 12524 and 13224 have impact hub deflections of around 10.01 mm and 10.00 mm respectively. These are just sufficient to meet the target. This does not mean they are failed designs. It means that they are a different design solution: they maintain service support and efficiency in spoke count while still meeting the minimum impact target.

**Table 12**. Results of impact

| Profile ID | Impact hub deflection | Margin above 10 mm target | Impact interpretation |
|---|---|---|---|
| 7376 | 14.54 mm | +4.54 mm | Strong impact-compliance profile |
| 7390 | 14.39 mm | +4.39 mm | Strong impact-compliance profile |
| 12524 | 10.01 mm | +0.01 mm | Barely satisfies target; support-biased |
| 13224 | 10.00 mm | ~0.00 mm | Barely satisfies target; strongest support-biased profile |

The impact results finish the analysis of the two families. The 14 mm installation-stretch family has greater impact travel and greater compliance margin. The 6 mm installation-stretch family has more service support and fewer spokes to reach the impact target. So, the design space does not yield a winner, it yields a compliance vs support trade-off. All results are shown in Table 12.

### 3.8. CAD Modelling of Profiles 7376 and 13224

To translate the reduced-order MATLAB results into geometry, two profiles were modelled in SolidWorks. The compliance-oriented was profile 7376, which had the largest impact hub-deflection margin. The support-oriented was profile 13224, which had the smallest service hub-deflection and 20 spokes (Table 13). Both CAD model designs can be observed in Fig. 21 and 22.

This is because the MATLAB screening process identifies mechanically promising sets of parameters, but it does not ensure that the geometry can be embodied as a physical part. The CAD embodiment process guarantees that the chosen set of parameters can be embodied as a physically realisable spoke-like geometry with tube regions, localised CFT regions and interfaces.

As a conclusion to the MATLAB screening process, the profiles with most available compliance and the profile providing most support were selected to be modelled in SolidWorks. The following process captures the static simulation and its impact on both profiles, as well as examination under buckling simulation setup to compare the out to the original full length CFT structure.

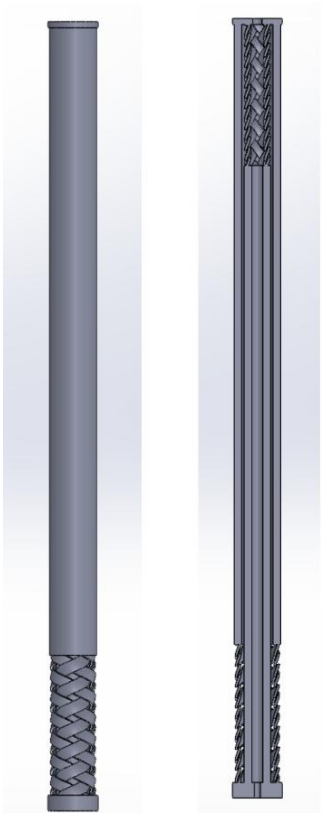

**Fig. 21.** CAD model for profile 7376

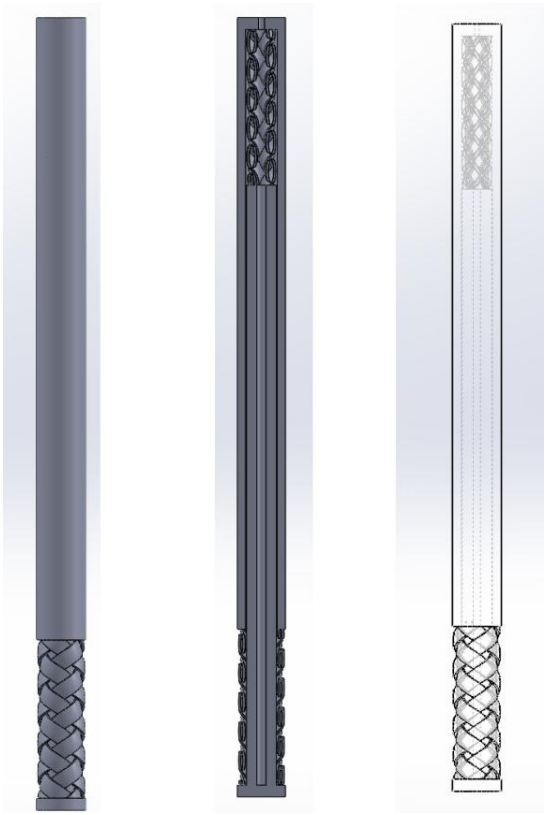

**Fig. 22.** CAD model for profile 13224

**Table 13**. Properties used for modelling of profiles 7376 and 13224

| **Parameter** | **Profile 7376** | **Profile 13224** |
|---|---|---|
| Design family | Compliance-oriented | Support-oriented |
| Hybrid coaxial design logic | Localised CFT region with coaxial structural support | Localised CFT region with coaxial structural support |
| Initial CFT height | 48 mm | 54 mm |
| Outer branch strip width | 5.0 mm | 6.0 mm |
| Inner branch strip width | 3.5 mm | 5.5 mm |
| Strip thickness | 0.8 mm | 0.8 mm |
| Turn count | 2.5 | 2.0 |
| Installation stretch | 14 mm | 6 mm |
| Tube material | Baseline tube | Baseline tube |
| Strip material | CFRP strip surrogate | CFRP strip surrogate |
| Interpretation | Higher installation stretch and larger motion reserve; selected as the compliance-oriented representative | Wider branch geometry and lower installation stretch; selected as the support-oriented representative |

### 3.9. Static Simulation of Profiles 7376 and 13224

Static simulation was used to perform a first-order component analysis of profiles 7376 and 13224. This was not to validate the final product, but to see if the MATLAB-selected profiles were structurally feasible when embodied in 3D CAD models.

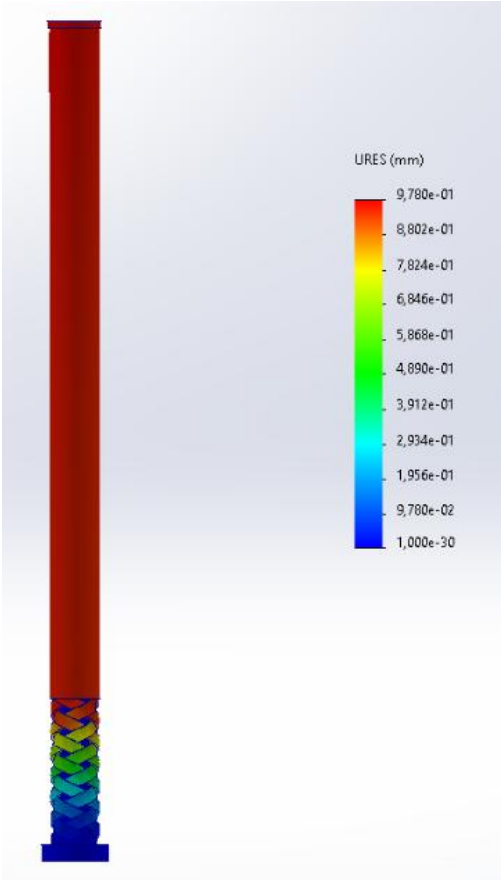


**Fig. 23.** Results of stress for profiles 7376

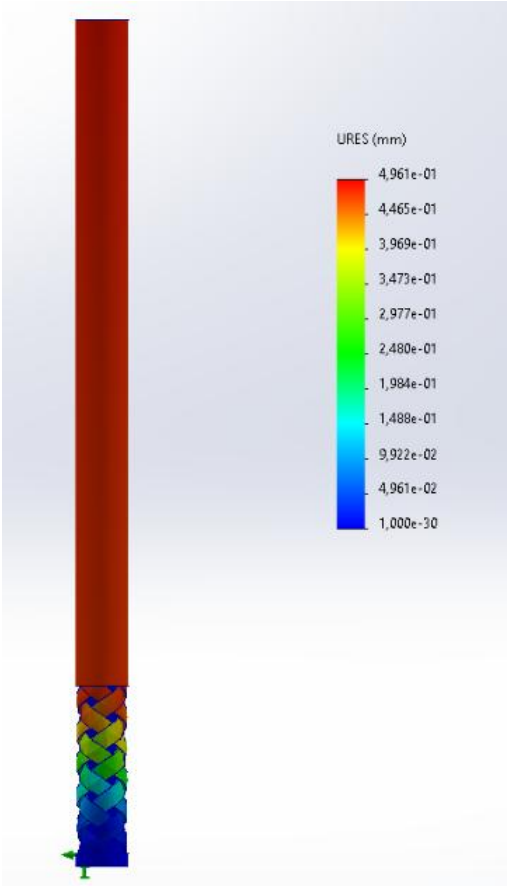


**Fig. 24.** Results of stress for profiles 13224

A static solid-mesh analysis was carried out in SolidWorks Simulation. The models were given a linear elastic isotropic material, Thornel Mat VMA, with elastic modulus $E$= 70 GPa, Poisson's ratio $\nu$ = 0.30, density 1600 kg/m³, and nominal yield strength $6.0\times10^{8}$ N/m². The static study was fixed at one end and had a 200 N normal force at the other end (Fig. 23 and 24). The interaction was bonded, localised interaction between straps was set to contact with friction coefficient of 0.15.

Profile 7376 produced a maximum resultant displacement of 0.978 mm, a maximum von Mises stress of $5.114\times10^{8}$ N/m², and a maximum equivalent strain of $4.297\times10^{-3}$. Its mass was 0.05394 kg. The mesh had 35.203 nodes and 16.365 elements.

Profile 13224 produced a lower maximum resultant displacement of 0.49 mm, a lower maximum von Mises stress of $3.517\times10^{8}$ N/m², and a lower maximum equivalent strain of $2.397\times10^{-3}$. Its mass was 0.06734 kg. The mesh had 47.956 nodes and 24.698 elements. Results of the stress and simulation for the two profiles are observed in Fig. 25 and 26.

The static analysis results show that both embodied profiles were below the nominal yield strength of the material in the simple linear static analysis. Profile 7376 has a maximum von Mises stress of

$5.114\times10^8$ N/m², giving a stress margin of 1.17 relative to the nominal yield strength of $6.0\times10^8$ N/m². Profile 13224 had a maximum von Mises stress of $2.182\times10^8$ N/m², resulting in a stress margin of 2.75.

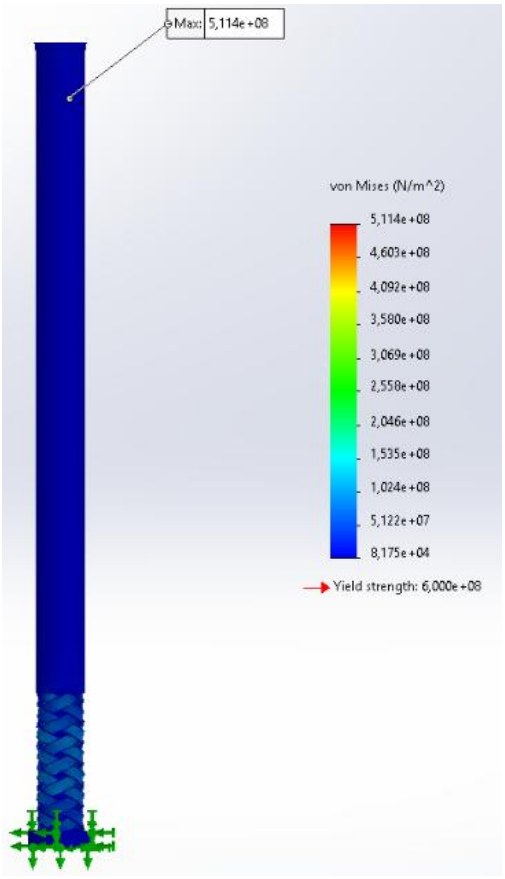


**Fig. 25.** Results of displacements for profiles 7376

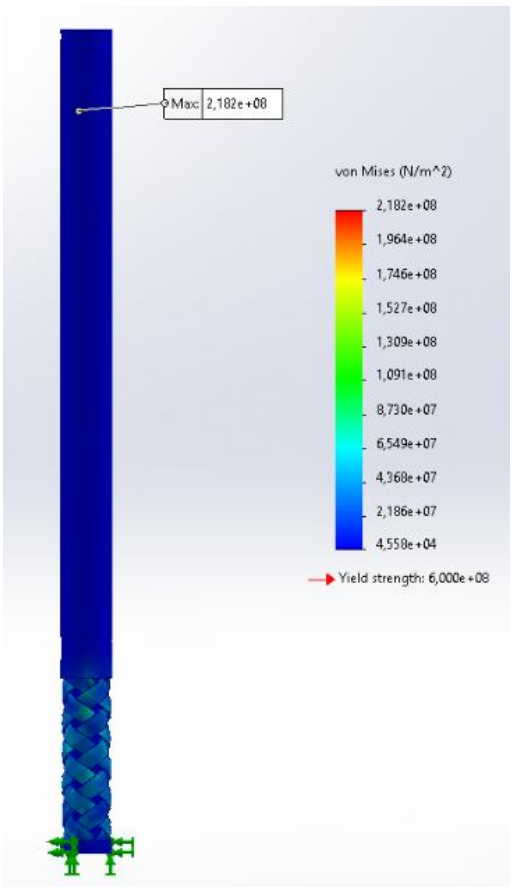


**Fig. 26.** Results of displacements for profiles 13224

When it comes to deformation, Profile 7376 has a maximum resultant displacement of 1.300 mm under the 200 N load, whereas profile 13224 has a maximum resultant displacement of 0.49 mm. This is consistent with the behaviour of the two design families. Profile 7376 is less stiff and therefore deforms more than profile 13224 under the same load.

The strain results follow the same trend. Profile 7376 has a maximum equivalent strain of $4.297\times10^{-3}$, profile 13224 has a maximum equivalent strain of $1.488\times10^{-3}$. The lower stress, displacement, and strain of profile 13224 indicate that it is the more conservative design in the static component-level simulation.

However, profile 7376 should not be dismissed. The higher displacement is expected for the compliance profile. The higher stress indicates a lower static margin, but it was still below the nominal yield strength under the assumptions of the simplified simulation. Therefore, the static simulation results show that profile 7376 is the compliance profile, and profile 13224 is the support profile.

Overall, the static simulation results indicate that both embodied profiles are feasible under the simplified component-level load case. Profile 7376 is more compliant, but has a lower stress margin. profile 13224 is stiffer, has lower stress and strain, and a higher stress margin, and is more conservative. These results confirm the thesis interpretation that the final design space does not

provide a single optimal profile, but two viable design alternatives: one that is more compliant, and one that is more supportive.

### 3.10. Buckling Simulation of Modelled Profiles

The candidates were assessed for buckling to see if they were stable under idealised component loads. The candidates were analysed using linear eigenvalue buckling in SolidWorks Simulation. The first five buckling modes were calculated with a reference load of 100 N.

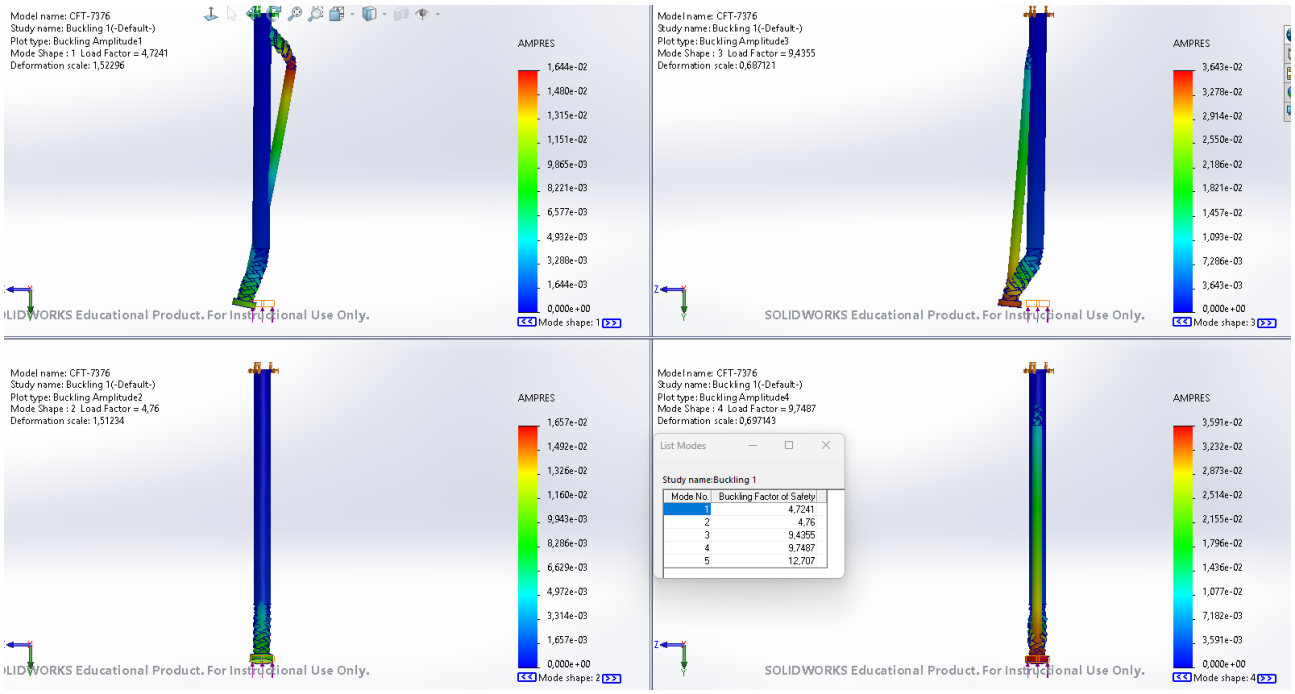


**Fig. 27.** Results for buckling for profile 7376

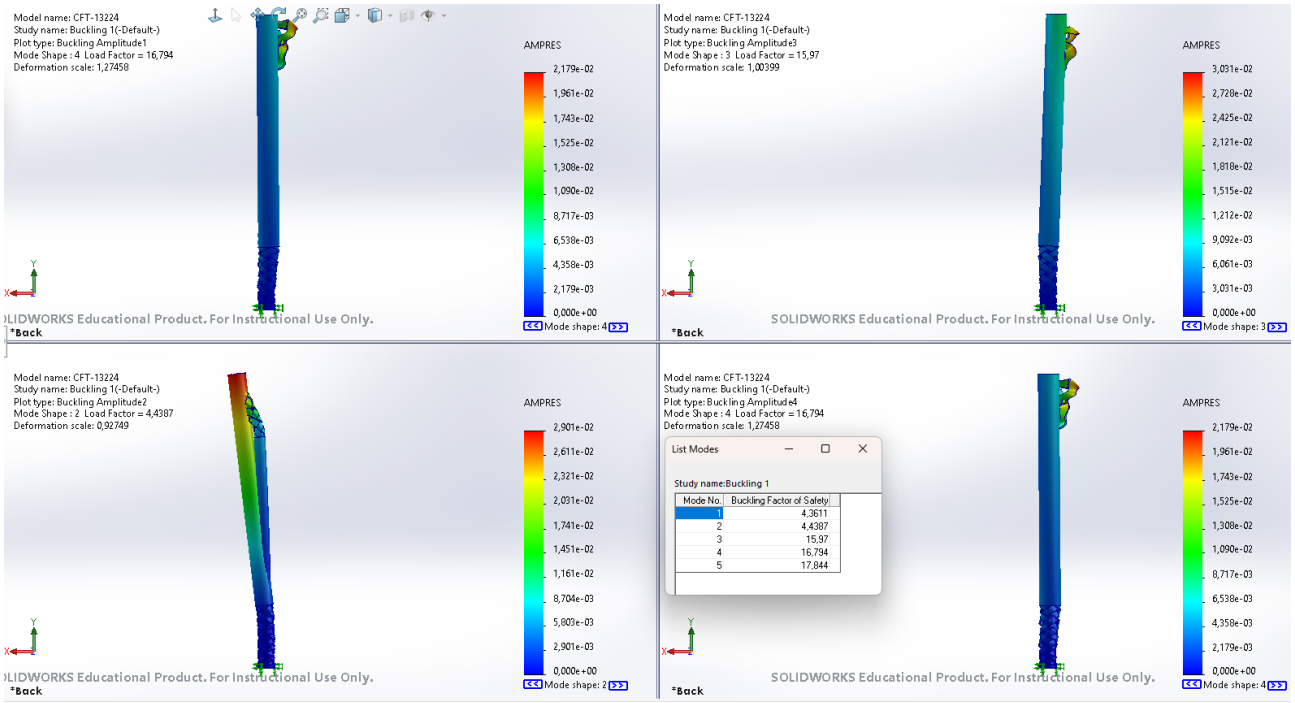


**Fig. 28.** Results for buckling for profile 13224

Candidate 7376 produced first five buckling load factors of 4.7241, 4.7600, 9.4355, 9.7487, and 12.707. The first buckling load factor was therefore 4.7241. This is an estimated ideal critical buckling load of 472.41 N with the 100 N reference load, can be seen in Fig. 27.

Candidate 13224 produced first five buckling load factors of 4.3611, 4.4387, 15.970, 16.794, and 17.844. The first buckling factor was thus 4.3611. This is an estimated ideal critical buckling load of 436.11 N for the 100 N reference load, as shown in Fig. 28.

The two embodied candidates easily passed the buckling stability test. Although 7376 had a higher first buckling factor, 13224 had a lower displacement and stress in the static analysis. So, the buckling factor is not the only consideration. Instead, all the results should be considered: 7376 has a higher compliance reserve and a slightly higher first buckling factor, but 13224 has a higher static support, lower stress, lower strain and lower service deflection. All simulation results presented in Table 14.

**Table 14**. Results of buckling for profiles 7376 and 13224

| **Result** | **Profile 7376** | **Profile 13224** |
|---|---|---|
| Applied reference load | 100 N | 100 N |
| First buckling load factor | 4.7241 | 4.3611 |
| Estimated first critical buckling load | 472.41 N | 436.11 N |
| Second buckling load factor | 4.7600 | 4.4387 |
| Third buckling load factor | 9.4355 | 15.970 |
| Fourth buckling load factor | 9.7487 | 16.794 |
| Fifth buckling load factor | 12.707 | 17.844 |
| Minimum required factor | 2.0 | 2.0 |
| Buckling criterion | Pass | Pass |

### 3.11. Final Comparison of Selected Profiles

The last comparison is between the MATLAB screening, CAD embodiment, static simulation and buckling simulation. Candidates 7376 and 13224 are both compliant designs and passed the MATLAB screening and embodied simulation tests, but they are not the same design.

Candidate 7376 is the better compliant design. It had the largest impact hub deflection of the embodied representatives, 14.54 mm predicted by the MATLAB screening. It also had a large lock margin of 20.87 mm. It is a good candidate for applications where the maximum impact travel and reserve compliance are critical. The better support design is Candidate 13224. It had the minimum number of 20 spokes in the MATLAB service screen, the minimum service hub deflection of the shortlisted candidates and lower displacement, stress and strain in static simulation. It just met the 10 mm impact limit, but with better service support.

This final comparison (Table 15) shows that the hybrid CFT spoke should not be marketed. It is better to consider the methodology has found two solutions. Candidate 7376 is preferred where compliance is the most important consideration. Candidate 13224 is better if service support, stress and spoke count are important. This is a better engineering result because it recognises the compliance-discipline trade-off.

**Table 15**. Comparison of profiles 7376 and 13224

| **Criterion** | **Profile 7376** | **Profile 13224** | **Preferred candidate** |
|---|---|---|---|
| Design family | Compliance-oriented | Support-oriented | Depends on objective |
| Installation stretch | 14 mm | 6 mm | — |
| Required spoke count | 28 | 20 | 13224 |
| Service hub deflection | 1.36 mm | 0.95 mm | 13224 |
| Impact hub deflection | 14.54 mm | 10.00 mm | 7376 |
| Lock margin | 20.87 mm | 10.21 mm | 7376 |
| Static displacement under 200 N | 1.300 mm | 0.791 mm | 13224 |
| Maximum von Mises stress | $5.114\times10^{8}$ N/m² | $2.182\times10^{8}$ N/m² | 13224 |
| Static stress margin | 1.17 | 2.75 | 13224 |
| First buckling factor | 4.7241 | 4.3611 | 7376 slightly |
| Overall interpretation | Larger compliance reserve | Stronger structural support | Trade-off |

## 3.12. Discussion Interpretation

The results show that the Chinese finger trap is a local compliant mechanism, not a full-length spoke. The RP2 full-length CFT results showed the mechanism, but also that full-length compliance results in stability and buckling problems. The first hybrid then showed that the second branch and second span is not enough: the branches must cooperate. The failure of the inner CFT after cyclic loading demonstrated that the load participation of the inner and outer compliant branches is important.

The final MATLAB screening solved this problem by screening the candidates with the displacement targets, but also with the installed state support, lock margin, branch force participation, service deflection, spoke count feasibility, buckling safety and impact response. That's why only four candidates were selected from 29.400 profiles. The small successful region is good news because it means that the final candidates were selected by engineering judgement.

The embodied simulations also support the approach. The static and buckling simulations demonstrate that the 7376 and 13224 candidates were feasible. The 7376 result shows that a compliance-oriented hybrid CFT spoke can deliver high impact travel while meeting the component-level stress and buckling requirements. The 13224 result demonstrates that a support-oriented hybrid CFT spoke can provide low impact travel and stress while satisfying the minimum impact-travel constraint. The two results demonstrate that the hybrid architecture can be tailored for different mechanical performance.

The thesis thus does not offer a productised spoke, but a technically robust design process. It begins with a validated CFT mechanism, identifies the structural weakness of the full-length spoke, uses experiments to identify branch-load imbalance in the hybrid architecture, screens the design space with MATLAB and then validates several candidates with CAD embodiment and component simulation.

### 3.13. Limitations of the Results

The findings need to be viewed in the light of the modelling and experiments. The MATLAB screening was a reduced-order model without local contact, friction, anisotropy, imperfections or the wheel. The SolidWorks simulations were linear elastic, simplified bonded contact, friction off, and large-displacement off. So, the static and buckling simulations are plausibility studies at the component level, not the product level.

The buckling results are also idealized. A linear eigenvalue buckling factor is the buckling load for an ideal model with the given boundary conditions. The specimens may buckle at lower loads because of imperfections, off-axis loads, local damage, contact, printing errors or material anisotropy. Therefore, the buckling factors of 7376 and 13224 are good relative stability indicators, but not the physical buckling loads.

The preliminary hybrid cyclic test is a good physical test for branch-load imbalance, but not the final fatigue test of the optimized candidates. The fatigue of the final candidates should be tested with the final design, final material system, controlled boundary conditions and multiple specimens. Nonlinear contact modelling, wheel testing and production-material testing are needed to complete the hybrid CFT spoke.

# 4. Economic Breakdown

## 4.1. Purpose of the Economic Breakdown

This chapter presents a prototype-level economic breakdown for the two embodied hybrid coaxial spoke profiles: candidate profile 7376 and candidate profile 13224. The purpose is not to estimate mass-production cost, but to compare the practical manufacturing effort required to prototype both selected designs by fused-filament 3D printing.

The economic comparison includes the mass of each spoke, required spoke count, total wheel-level mass, Cura printing time, material consumption, support material, calculated machine hourly rate, designer labour, and 3D printer operator labour. Candidate profile 7376 represents the compliance-oriented design direction, while candidate profile 13224 represents the support-oriented design direction.

## 4.2. Machine Hourly Rate Calculation

The machine hourly rate was calculated instead of being assumed directly. The printer used for the estimate was an Ultimaker S5. The machine cost was calculated using printer depreciation, annual maintenance allowance, electricity consumption, and laboratory overhead.

The Ultimaker S5 has a listed gross price of 6.543,81 € and a maximum power output of 500 W. The electricity price used for Lithuania was 0,107 €/kWh for business electricity. Data are shown in Table 16.

MHR was calculated as per equation (45):

$$MHR = \left(\frac{C_{\text{printer}}}{L \cdot H_{\text{annual}}} + \frac{C_{\text{maintenance,annual}}}{H_{\text{annual}}} + P_{\text{printer}} \cdot C_{\text{electricity}}\right) \cdot (1 + f_{\text{overhead}}), \quad (45)$$

where $C_{printer}$ is the printer purchase cost, $L$ is the assumed service life, $H_{annual}$ is the annual productive machine time, $P_{pritner}$ is the printer power demand and $f_{overhead}$ is the laboratory overhead factor.

**Table 16**. Data used for calculations

| Parameter | Symbol | Value |
|---|---|---|
| Printer purchase cost | $C_{printer}$ | 6.543,81 € |
| Service life | $L$ | 5 years |
| Annual productive machine time | $H_{annual}$ | 1.000 h/year |
| Annual maintenance allowance | 0,10 $C_{printer}$ | 654,38 €/year |
| Printer power demand | $P_{printer}$ | 0,5 kW |
| Electricity price | $C_{electricity}$ | 0,107 €/kWh |
| Laboratory overhead factor | $f_{overhead}$ | 20% |

The depreciation cost per machine hour is given by equation (46):

$$C_{\text{depreciation,h}} = \frac{C_{\text{printer}}}{L \cdot H_{\text{annual}}} = \frac{6543.81}{5 \times 1000} = 1.31\ €/\text{h}, \quad (46)$$

The maintenance cost per machine hour is given by equation (47):

$$C_{\text{maintenance,h}} = \frac{C_{\text{maintenance,annual}}}{H_{\text{annual}}} = \frac{654.38}{1000} = 0.65\ €/\text{h}. \quad (47)$$

The electricity cost per machine hour is given by equation (48):

$$C_{\text{electricity,h}} = P_{\text{printer}} \cdot C_{\text{electricity}} = 0.5 \times 0.107 = 0.05\ €/\text{h}. \quad (48)$$

Therefore, before overhead, MHR is expressed by equation (49):

$$MHR_{\text{base}} = C_{\text{depreciation,h}} + C_{\text{maintenance,h}} + C_{\text{electricity,h}} = 1.31 + 0.65 + 0.05 = 2.02\ €/\text{h}. \quad (49)$$

Including 20% overhead laboratory, the final MHR is given by equation (50):

$$MHR = MHR_{\text{base}} \cdot (1 + f_{\text{overhead}}) = 2.02 \times 1.20 = 2.42\ €/\text{h}. \quad (50)$$

### 4.3. Input Values Used for Cost Estimation

The Cura estimates were obtained with two spokes placed on one print bed. Therefore, one print cycle produces two spokes. Candidate profile 7376 requires 28 spokes per wheel, corresponding to 14 print cycles. Candidate profile 13224 requires 20 spokes per wheel, corresponding to 10 print cycles.

With the prototype manufacturing input values given in Table 17. The mass and time for print data can be seen in Figures 29 and 30.

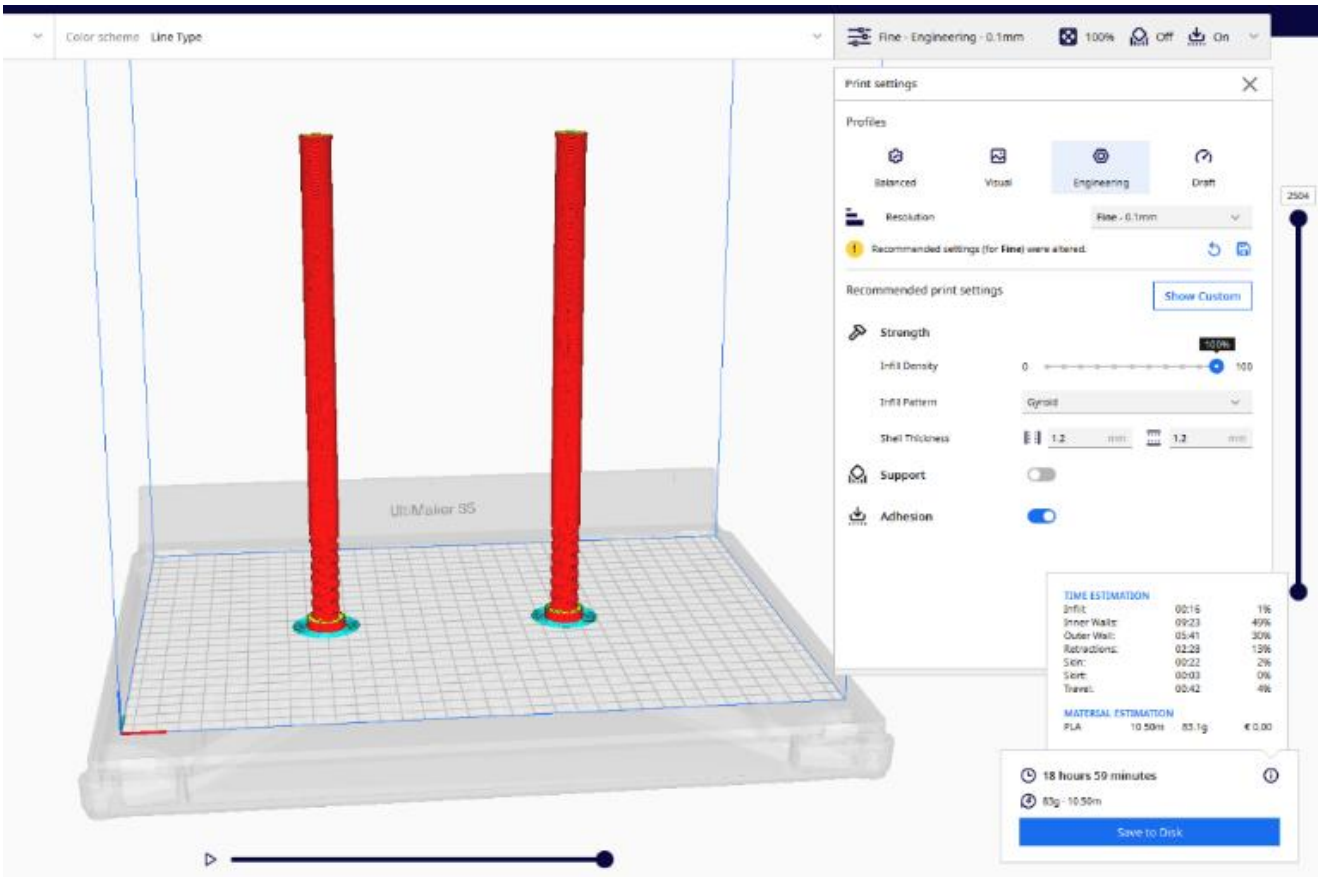


**Fig. 29.** The mass and time data for printing profile 7376

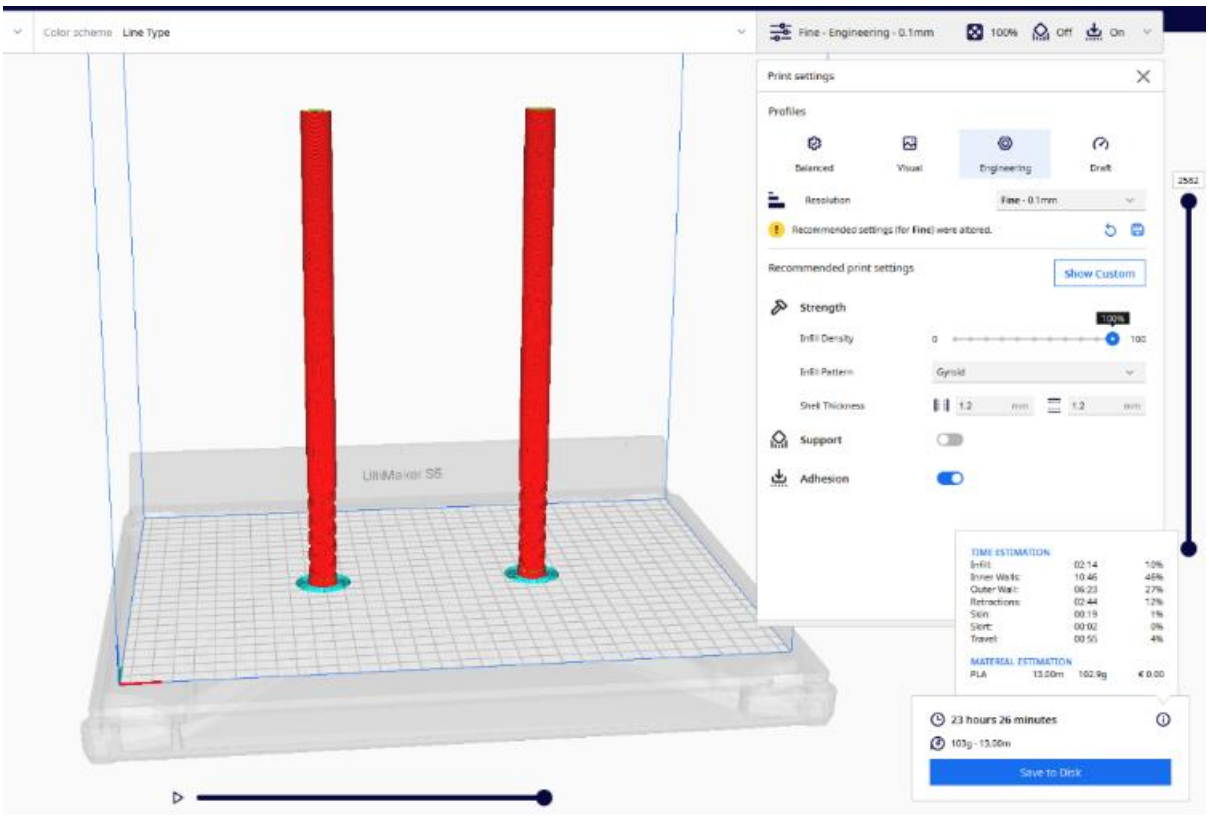


**Fig. 30.** The mass and time data for printing profile 13224

**Table 17.** Input values

| **Parameter** | **Profile 7376** | **Profile 13224** |
|---|---|---|
| Design direction | Compliance-oriented | Support-oriented |
| CAD mass per spoke | 53,94 g | 67,34 g |
| Required spoke count | 28 | 20 |
| CAD total spoke mass per wheel | 1,510 kg | 1,347 kg |
| Spokes printed per bed | 2 | 2 |
| Number of print cycles | 14 | 10 |
| Cura print time per cycle | 18 h 59 min | 23 h 26 min |
| Cura material per cycle, without support | 83,1 g | 102,9 g |
| Assumed support material per cycle | 70,0 g | 83,0 g |
| Calculated MHR | 2,42 €/h | 2,42 €/h |

## 4.4. Mass and Material Consumption

The final wheel level spoke mass was calculated using equation (51):

$$m_{\text{wheel}} = m_{\text{spoke}}.n. \tag{51}$$

For profile 7376:

$$m_{\text{wheel}} = m_{\text{spoke}}.n = 0.05394 \times 28 = 1.510\,\text{kg}.$$

For profile 13224:

$m_{\text{wheel}} = m_{\text{spoke}}.n = 0.06734 \times 20 = 1.347\,\text{kg}.$

The total consumed printing material includes both the Cura material estimate and the support material is:

$$m_{\text{printed,total}} = \left(m_{\text{Cura,cycle}} + m_{\text{support,cycle}}\right).N_{\text{cycles}}. \quad (52)$$

$m_{\text{printed,total,7376}} = (0.0831 + 0.0700) \times 14 = 2.143\,\text{kg}.$

$m_{\text{printed,total,13224}} = (0.1029 + 0.0830) \times 10 = 1.859\,\text{kg}.$

Table 18 shows data on mass and material consumption.

**Table 18.** Data on mass and material consumptions

| **Parameter** | **Profile 7376** | **Profile 13224** |
|---|---|---|
| Cura material per print cycle | 83,1 g | 102,9 g |
| Support material per print cycle | 70,0 g | 83,0 g |
| Total material per print cycle | 153,1 g | 185,9 g |
| Number of print cycles | 14 | 10 |
| Total Cura material, without support | 1,163 kg | 1,029 kg |
| Total support material | 0,980 kg | 0,830 kg |
| Total consumed printing material | 2,143 kg | 1,859 kg |

Candidate profile 13224 requires less total consumed material at wheel level because it requires fewer spokes, even though each individual spoke is heavier.

### 4.5. Printing Time and Machine Cost

The total machine cost was calculated as per equations (53) and (54),

$$t_{\text{print,total}} = t_{\text{cycle}} \cdot N_{\text{cycles}}, \quad (53)$$

$$C_{\text{machine}} = t_{\text{print,total}}.MH\text{R}. \quad (54)$$

For profile 7376:

$t_{\text{print,total,7376}} = 18.983 \times 14 = 265.77\,\text{h},$

$C_{\text{machine,7376}} = 265.77 \times 2.42 = 643.15\,€.$

And for profile 13224:

$t_{\text{print,total,13224}} = 23.433 \times 10 = 234.33\,\text{h},$

$C_{\text{machine,13224}} = 234.33 \times 2.42 = 567.09\,€.$

Print time and machine cost are shown in Table 19.

**Table 19.** Print time and machine cost

| Parameter | Candidate profile 7376 | Candidate profile 13224 |
|---|---|---|
| Print time per cycle | 18,98 h | 23,43 h |
| Number of print cycles | 14 | 10 |
| Total print time | 265,77 h | 234,33 h |
| Calculated MHR | 2,42 €/h | 2,42 €/h |
| Machine cost | 643,15 € | 567,09 € |

Although candidate profile 13224 has a longer print time per cycle, it requires fewer print cycles. Therefore, its total print time and machine cost are lower.

### 4.6. Labour Cost

The design time for preparing both spoke profiles was taken as 4 h in total. Since two profiles were designed, 2 h was allocated to each candidate profile.

The designer hourly rate was estimated from the Lithuanian average gross monthly salary of 2.526,8 €/month, divided by 173,3 working hours/month. The 3D printer operator's hourly rate was taken as the Lithuanian minimum hourly wage of 7,05 €/h. Designers' and operators' hourly time and cost are calculated using Equations (55) – (58) and presented in Table 20.

$$R_{\text{designer}} = \frac{S_{\text{monthly}}}{H_{\text{monthly}}}, \tag{55}$$

$$R_{\text{designer}} = \frac{2526.8}{173.3} = 14.58\,€/\text{h}.$$

$$C_{\text{designer}} = t_{\text{designer}} \cdot R_{\text{designer}}, \tag{56}$$

$$C_{\text{designer}} = 2 \times 14.58 = 29.16\,€.$$

$$t_{\text{operator,total}} = N_{\text{cycles}} \cdot t_{\text{operator,cycle}}, \tag{57}$$

$$t_{\text{operator,7376}} = 14 \times 0.5 = 7\,\text{h},$$

$$t_{\text{operator,13224}} = 10 \times 0.5 = 5\,\text{h}.$$

$$C_{\text{operator}} = t_{\text{operator,total}} \cdot R_{\text{operator}}, \tag{58}$$

$$C_{\text{operator,7376}} = 7 \times 7.05 = 49.35\,€,$$

$$C_{\text{operator,13224}} = 5 \times 7.05 = 35.25\,€.$$

**Table 20.** Data of labour cost

| Parameter | Profile 7376 | Profile 13224 |
|---|---|---|
| Allocated designer time | 2 h | 2 h |
| Designer hourly rate | 14,58 €/h | 14,58 €/h |
| Designer cost | 29,16 € | 29,16 € |

| | | |
|---|---|---|
| Operator time per print cycle | 0,5 h | 0,5 h |
| Total operator time | 7 h | 5 h |
| Operator hourly rate | 7,05 €/h | 7,05 €/h |
| Operator cost | 49,35 € | 35,25 € |

### 4.7. Total Prototype Cost

The total prototype cost was calculated by combining material cost, machine cost, designer labour cost, and 3D printer operator cost. Since the proposed spoke is intended as a carbon-fibre-reinforced prototype rather than a standard PLA spoke, the material cost was calculated using a CFRP/CF-PLA filament price. For FDM printing, this should be interpreted as a carbon-fibre-reinforced printing filament surrogate, not as continuous-fibre structural CFRP laminate. European supplier prices for carbon-fibre-reinforced filaments vary, with examples such as Bambu Lab PLA-CF at approximately 26,70–28,70 €/kg, Polymaker PLA-CF at approximately 35,70 €/kg, and Spectrum Carbon PLA at approximately 44,80 €/kg. Therefore, a rounded conservative material cost of 45 €/kg was used for the prototype calculation.

Material cost is found from equation (59):

$$C_{\text{material}} = m_{\text{printed,total}} \cdot C_{\text{material,kg}}, \tag{59}$$

$$C_{\text{material,7376}} = 2.143 \times 45 = 96.44\,€,$$

$$C_{\text{material,13224}} = 1.859 \times 45 = 83.66\,€.$$

Total cost calculated as shown in equation (60):

$$C_{\text{total}} = C_{\text{material}} + C_{\text{machine}} + C_{\text{designer}} + C_{\text{operator}}, \tag{60}$$

$$C_{\text{total,7376}} = 53.59 + 643.15 + 29.16 + 49.35 = 818.1\,€,$$

$$C_{\text{total,13224}} = 46.48 + 567.09 + 29.16 + 35.25 = 715.16\,€.$$

The summarized results are presented in Table 21.

**Table 21.** Total cost

| **Cost item** | **Profile 7376** | **Profile 13224** |
|---|---|---|
| Total consumed printing material | 2,143 kg | 1,859 kg |
| CFRP/CF-PLA material cost | 45 €/kg | 45 €/kg |
| Material cost | 96,44 € | 83,66 € |
| Machine cost | 643,15 € | 567,09 € |
| Designer cost | 29,16 € | 29,16 € |
| Operator cost | 49,35 € | 35,25 € |
| Total prototype cost per wheel | 818,10 € | 715,16 € |

## 5. Discussion

The current hybrid coaxial spoke is a more structurally disciplined, but heavier and more complicated alternative to the full-length CFT spoke of RP2. The full-length CFT was light and had high mechanism-level compliance, with about 9.0 mm hub deflection in the comparative wheel simulation, and progressive stiffening/lock-up experimentally. But it relied on the full span of the spoke to be compliant, which was susceptible to instability and buckling. The hybrid design trades-off simplicity and weight efficiency to confine the CFT mechanism and add coaxial support. Thus, the final hybrid profiles achieve more wheel-relevant considerations that were not met by the full-length CFT alone, such as support in the installed state, service deflection, branch participation, spoke count, and buckling. Profile 7376 is the higher-compliance extension of the CFT concept, and profile 13224 is the more support-oriented and prototype-friendly profile. All above mentioned results are presented in Table 22.

**Table 22.** Data summary

| **Criterion** | **RP2 full-length CFT** | **Hybrid profile 7376** | **Hybrid profile 13224** |
|---|---|---|---|
| Design role | Mechanism proof-of-concept | Compliance-oriented final candidate | Support-oriented final candidate |
| Compliance location | Entire spoke span | Localised CFT region | Localised CFT region |
| Structural architecture | Full-length helical CFT lattice | CFT region + coaxial support span | CFT region + coaxial support span |
| Main design purpose | Validate CFT nonlinear mechanism | Maximise compliant travel while passing screening | Improve support, reduce service deflection, reduce spoke count |
| Spoke/wheel configuration used | 7 CFT spokes in simplified wheel model | 28-spoke wheel configuration | 20-spoke wheel configuration |
| CAD/FEA spokes-only mass | 210 g in RP2 wheel model | 1.510 kg per wheel | 1.347 kg per wheel |
| Individual spoke CAD mass | Not directly reported in final RP2 matrix | 53.94 g | 67.34 g |
| Printed prototype material | 75 g total; 52 g structure + 23 g support | 2.143 kg total consumed material per wheel | 1.859 kg total consumed material per wheel |
| Wheel-level / impact deflection | ~9.0 mm hub deflection in RP2 FEA; ~11 mm MATLAB estimate | 14.54 mm impact hub deflection | 10.00 mm impact hub deflection |
| Service hub deflection | Not part of final hybrid service screen | 1.36 mm | 0.95 mm |
| Lock-up / stiffening behaviour | Experimental lock-up after ~37.5 mm | 20.87 mm lock margin | 10.21 mm lock margin |
| Buckling behaviour | Vulnerable; lowest relevant positive factor ~0.3383 | First buckling factor 4.7241 | First buckling factor 4.3611 |
| Static stress margin | Not final candidate check | 1.17 | 1.71 / higher support margin, depending final FEA setup |
| Estimated prototype cost per wheel | Not costed in RP2; print mass only available | 818.10 € using CFRP/CF-PLA estimate | 715.16 € using CFRP/CF-PLA estimate |

| | | | |
|---|---|---|---|
| Main advantage | Light, simple, validated nonlinear CFT mechanism | Highest compliance reserve and impact deflection | Best service support, lower spoke count, lower total cost |
| Main limitation | Whole-span compliance caused poor structural discipline and buckling vulnerability | Higher total mass, higher stress, higher spoke count | Barely exceeds 10 mm impact target |
| Final interpretation | Mechanism validated, architecture not sufficient as final spoke | Best compliance continuation | Best support/economic continuation |

The cost and mass figures should not be viewed as a commercial comparison since the full-length CFT was a design exercise concept only, but the hybrid profiles were assessed as potential wheel-relevant prototypes with various service, buckling, spoke-count, and cost goals.

The final recommended architecture is Profile 13224, which has the following advantages: meets the required 10 mm deflection at impact, has improved service-state control, lower static displacement, lower stress concentration, is feasible for 20-spoke implementation and has better support-oriented behaviour. Profile 7376 is retained as an alternate option for future development for compliance if a larger impact travel is desired.

This study is for architectural validation and NOT the final commercial wheel validation. The experimental study confirms the nonlinear CFT mechanism behaviour and confirms the branch-load participation as an important design requirement. The optimised profiles are then tested with reduced order screening and component-level simulation. So, final full wheel dynamic testing does not replace the current thesis contribution, but is seen as the next step in the dynamic validation process.

## Conclusions

1. A series of wheel-spoke component design acceptance criteria, loadings, test plan and evaluation metrics were established to evaluate the proposed compliant spoke as an in-wheel suspension. The design was assessed for an 80 kg bicycle-rider, 450 N service design load, safety factor of 1.5 and a screened service load of 675 N. The key performance requirement was deemed to be a minimum of 10 mm radial deflection of the hub, with a maximum allowable deflection of 2.50 mm in a service condition to retain the wheel shape. Other acceptance criteria for the design included minimum service force retention, maximum installed pretension, number of spokes, branch force participation and minimum buckling safety factor. This enabled the design to be assessed not just as a compliant mechanism, but also as a spoke-like structure that had to be compliant (deflectable) as well as being stable.
2. A novel coaxial compliant spoke design was created and parametrised in a CAD model for manufacturing. The final design transformed the previous successful Chinese finger trap (CFT) compliant mechanism design from a compliant strip to a localised compliant CFT region and coaxial tube section. This design had two branches in parallel and the CFT and tube sections were in series. The design variables of the CFT (CFT length, branch strip widths, strip thickness, turn count, installation stretch, and material) formed a design space of 29,400 profiles. Four candidate profiles that met the thesis success criteria were chosen, and two - 7376 and 13224 - were CAD designed for comparison.
3. The design was optimised and validated using MATLAB screening and SolidWorks component simulation. The MATLAB screening reduced 29.400 profiles to four successful profiles, according to geometric, installed state, service state, number of spokes, buckling and impact-response constraints. profile 7376 modelled in the compliant design direction, with 14.54 mm impact hub deflection and 20.87 mm margin to lock. Candidate profile 13224 embodied the support design direction with 0.95 mm service hub deflection, 10.00 mm impact hub deflection and 20 spokes. Static simulation of the embodied candidates suggested that both showed less than the selected nominal yield stress under the simplified component load case and buckling analysis suggested first buckling factors greater than the minimum. Thus, the hybrid design reached the first order strength and stability goals, as per the static simulations under the simplifying assumptions.
4. Phototypes were manufactured and tested to experimentally validate the CFT-based compliant mechanism and explore possible failure modes in the hybrid design. The prior full-length CFT prototype validated the expected nonlinear, hardening, and locking behaviour, however, it also revealed that the CFT mechanism across the full length of the spoke led to instability and buckling. The first hybrid prototype was designed to demonstrate the feasibility of the hybrid design concept for manufacturing and testing, but the post-test analysis revealed poor branch-level force participation: the inner CFT was activated early and failed before the outer CFT started. This encouraged the subsequent MATLAB screening by suggesting the branch-force participation and load-balance criteria. Thus, the experimental work provided physical feedback for the design but final wheel tests are needed for optimised 7376 and 13224 designs to be fully validated.
5. The final candidates for hybrid coaxial spoke were compared against the previous full-length compliant full-tubular (CFT) and precedent compliant wheels, and a coarse economic analysis was performed for a prototype. The hybrid concept sacrificed some simplicity in comparison to the full-length CFT, but provided more wheel-relevant design control in the form of localised

compliance, improved support, spoke count feasibility and higher buckling load (strength). Candidate 7376 was assessed as the more compliant design, with candidate 13224 assessed as the more supportive, cost-effective design. The economic evaluation found candidate 13224 had fewer spokes, lower total print time, lower total material cost, lower wheel-level spoke mass and estimated cost to produce a prototype than candidate 7376. So, the output of this thesis is not a commercialised wheel spoke design, but a validated design process from the validated CFT mechanism to the hybrid coaxial spoke architecture, including screening, CAD, simulation, experiments and cost-manufacturing analysis.

## List of References


1. MEIJAARD, J. P.; PAPADOPOULOS, J. M.; RUINA, A., and SCHWAB, A. L. Linearized dynamics equations for the balance and steer of a bicycle: a benchmark and review. *Proceedings of the Royal society A: mathematical, physical and engineering sciences*, t. 463 (2007), nr. 2084, p. 1955–1982. Available from: https://api.istex.fr/ark:/67375/V84-JQTVRVC2-7/fulltext.pdf.
2. BRANDT, J. *The bicycle wheel*. 3rd ed. California: AVOCET, Inc. PALO ALTO, 2003.
3. BURGOYNE, C. J. and DILMAGHANIAN, R. Bicycle wheel as prestressed structure. *Journal of Engineering Mechanics*, vol. 119 (1993), no. 3, p. 439–455. Available from: https://doi.org/10.1061/(ASCE)0733-9399(1993)119:3(439).
4. LÉPINE, J.; CHAMPOUX, Y., and DROUET, J. Road bike comfort: on the measurement of vibrations induced to cyclist. *Sports Engineering*, vol. 17 (2014), no. 2, p. 113–122. Available from: https://link.springer.com/article/10.1007/s12283-014-0168-9.
5. ROTHHÄMEL, M. Measuring vertical tyre stiffness of bicycle tyres. In: Bicycle and Motorcycle Dynamics 2023: *Symposium on the Dynamics and Control of Single Track Vehicles*, 18–20 October 2023, Delft University of Technology, Delft, Netherlands, 2023. Available from: https://doi.org/10.24404/63FD130DDF639DBECB55E672.
6. LÉPINE, J.; CHAMPOUX, Y. and DROUET, J. The relative contribution of road bicycle components on vibration induced to the cyclist. *Sports Engineering*, vol. 18 (2015), no. 2, p. 79–91. Available from: https://doi.org/10.1007/s12283-014-0168-9.
7. LÉPINE, J.; CHAMPOUX, Y. and DROUET, J. A laboratory excitation technique to test road bike vibration transmission. *Experimental Techniques*, vol. 40 (2016), no. 1, p. 227–234. Available from: https://doi.org/10.1007/s40799-016-0026-8.
8. MÍNGUEZ, J. M. and VOGWELL, J. An analytical model to study the radial stiffness and spoke load distribution in a modern racing bicycle wheel. *Proceedings of the Institution of Mechanical Engineers, Part C: Journal of Mechanical Engineering Science*, vol. 222 (2008), no. 4, p. 563–576. Available from: https://doi.org/10.1243/09544062jmes802.
9. SALAMON, N. J. and OLDHAM, R. A. Analysis for design of spoked bicycle wheels. *Finite Elements in Analysis and Design*, vol. 10 (1992), no. 4, p. 319–333. Available from: https://www.sciencedirect.com/science/article/pii/0168874X92900199.
10. GAVIN, H. P. Bicycle-wheel spoke patterns and spoke fatigue. *Journal of Engineering Mechanics*, vol. 122 (1996), no. 8, p. 736–742.
11. HOWELL, L. L. Compliant Mechanisms. *The 2012 NSF Workshop* (2013) NSF Workshop, pp. 189–216. Available from: https://doi.org/10.1007/978-1-4471-4510-3.
12. ARREDONDO-SOTO, M.; CUAN-URQUIZO, E., and GÓMEZ-ESPINOSA, A. A review on tailoring stiffness in compliant systems, via removing material: *Cellular materials and topology optimization. Applied Sciences*, vol. 11 (2021), no. 8, p. 3538. Available from: https://doi.org/10.3390/app11083538.
13. CORNO, M.; PANZANI, G.; CATENARO, E., and SAVARESI, S. M. Modeling and analysis of a bicycle equipped with in-wheel suspensions. *Mechanical Systems and Signal Processing*, vol. 155 (2021), p. 107548. Available from: https://www.sciencedirect.com/science/article/pii/S0888327020309341.
14. NETI, A.; BRUNSWICK, A.; MARSALKO, L.; SHEARER, C., and KOONTZ, A. Effects of In-Wheel Suspension on Whole-Body Vibration and Comfort in Manual Wheelchair Users.

*Vibration*, vol. 7 (2024), no. 2, p. 432–452. Available from: https://doi.org/10.3390/vibration7020023.

15. Loopwheels. *Loopwheels urban, extreme and LT user manual*. Web site. Available from: https://loopwheels.com. [viewed 2026-03-26]
16. SoftWheel. *Wheelchairs powered by SoftWheel: Introducing the NEW SoftWheel 3*. Web site. Available from: https://www.softwheel.technology/technology. [viewed 2026-02-25].
17. Spinergy. *Unique PBO spokes that are ultralight and tough as nails*. Web site. Available from: https://bicycle.spinergy.com/. [viewed 2026-02-25].
18. Berd Spokes. *Technology overview - UHMWPE Bicycle Spokes*. Web site. Available from: https://berdspokes.com/pages/technology [viewed 2026-03-14].
19. Escape. *Diving deep: reviewing Berd polymer vs steel-bladed spokes*. Web site. Available from: https://escapecollective.com/ [viewed 2026-02-23].
20. HOU, S.; ZHAO, J., and YUREVICH, M. S. Design and analysis of a wheel with flexible spokes. *International Symposium on Multibody Systems and Mechatronics* (2017), p. 528–548. Available from: https://doi.org/10.1007/978-3-319-67567-1_50.
21. SHUAI, Z.; GAO, S.; YU, Y.; ZHAO, X.; YANG, W., and others. Characteristic study and design factor analysis of a novel non-pneumatic tyre with V-shaped spokes. *Materials & Design*, vol. 238 (2024), p. 112681. Available from: https://www.sciencedirect.com/science/article/pii/S0264127524000534.
22. DIXON, M. D.; O'DONNELL, M. P.; PIRRERA, A., and CHENCHIAH, I. V. Bespoke extensional elasticity through helical lattice systems. *Proceedings of the Royal Society A: Mathematical, Physical and Engineering Sciences*, vol. 475 (2019), no. 2232. Available from: https://doi.org/10.1098/rspa.2019.0547.
23. CAREY, S.; MCHALE, C., and WEAVER, P. M. A variable-topology morphing composite cylindrical lattice. *Composite Structures*, vol. 276 (2021), p. 114542. Available from: https://www.sciencedirect.com/science/article/pii/S0263822321010047.
24. CAREY, S.; MCHALE, C.; OLIVERI, V. and WEAVER, P. M. Reconfigurable multi-stable helical lattice. *Smart Materials, Adaptive Structures and Intelligent Systems*, vol. 84027 (2020), p. V001T01A001. Available from: https://doi.org/10.1115/SMASIS2020-2202.
25. CAREY, S.; MCHALE, C.; OLIVERI, V., and WEAVER, P. M. Reconfigurable helical lattices via topological morphing. *Materials & Design*, vol. 206 (2021), p. 109769. Available from: https://www.sciencedirect.com/science/article/pii/S0264127521003221.
26. QUAGLIERINI, J.; ARROYO, M., and DESIMONE, A. Mechanics of tubular meshes formed by elastic helical fibers. *International Journal of Solids and Structures*, vol.282 (2023), p. 112451. Available from: https://www.sciencedirect.com/science/article/pii/ S0020768323003487.
27. LU, D.; YOU, Z.; LIU, Z., and LU, G. The geometry and mechanics of the Chinese finger trap. *Extreme Mechanics Letters*, vol. 71 (2024), p. 102200. Available from: https://www.sciencedirect.com/science/article/pii/S2352431624000804.
28. SHAH, P. and SKIEDRAITĖ, I. Compliant Mechanism as Bicycle *Spokes. Mechanika 2025: Proceedings of the 29th International Scientific Conference* (2025). Available from: https://ebooks.ktu.edu/product/677423.
29. MAQSOOD, N. and RIMAŠAUSKAS, M. Characterization of carbon fiber reinforced PLA composites manufactured by fused deposition modeling. *Composites Part C: Open Access*, vol.

4 (2021), p. 100112. Available from: https://www.sciencedirect.com/science/article/pii/S2666682021000074.

30. WANG, A.; TANG, X.; ZENG, Y.; ZOU, L.; BAI, F., and others. Carbon fiber-reinforced PLA composite for fused deposition modeling 3D printing. *Polymers*, vol. 16 (2024), no. 15, p. 2135. Available from: 10.3390/polym16152135.
31. TOYOBO CO. Ltd. *Pro fiber ZYLON® (PBO Fiber) Technical Information*. Web site. Available from: https://www.toyobo.co.jp/. [viewed 2026-03-25].
32. TORAY. *TORAYCA™ T700G Standard Modulus Carbon Fiber Data Sheet*. Web site. Available from: https://www.toraycma.com/. [viewed 2026-03-25].
33. Dyneema. *Selecting the right fiber for mooring lines.* Web site. Available from: https://www.dsm.com/. [viewed 2026-03-27].
34. WANG, E. L. and HULL, M. L. A model for determining rider induced energy losses in bicycle suspension systems. *Vehicle System Dynamics*, vol. 25 (1996), no. 3, p. 223–246. Available from: https://doi.org/10.1080/00423119608968966.
35. NIELENS, H. and LEJEUNE, T. Bicycle shock absorption systems and energy expended by the cyclist. *Sports Medicine*, vol. 34 (2004), no. 2, p. 71–80.
36. THOMAS, T. L.; VENKITESWARAN, V. K.; ANANTHASURESH, G. K., and MISRA, S. A Monolithic compliant continuum manipulator: a proof-of-concept study. *Journal of mechanisms and robotics*, vol. 12 (2020), no. 6, p. 061006. Available from: https://doi.org/10.1115/1.4046838.
37. THOMAS, T. L.; KALPATHY VENKITESWARAN, V.; ANANTHASURESH, G. K., and MISRA, S. Surgical applications of compliant mechanisms: A review. *Journal of mechanisms and robotics,* vol. 13 (2021), no. 2, p. 020801. Available from: https://doi.org/10.1115/1.4049491.